Centromere deletion in *Cryptococcus deuterogattii* leads to neocentromere formation and chromosome fusions

Klaas Schotanus and Joseph Heitman*

Department of Molecular Genetics and Microbiology, Duke University Medical Center,

322 CARL Building, Box 3546, Research Drive, Durham, NC 27710 USA

*Corresponding author

Email: heitm001@duke.edu, Phone: +1-919-684-2824, Fax: +1-919-684-5458

Running title: Neocentromere formation in *Cryptococcus deuterogattii*

Abstract

The human fungal pathogen *Cryptococcus deuterogattii* is RNAi-deficient and lacks active transposons in its genome. *C. deuterogattii* has regional centromeres that contain only transposon relics. To investigate impact of centromere loss on the *C. deuterogattii* genome, either centromere 9 or 10 was deleted. Deletion of either centromere resulted in neocentromere formation and interestingly, the genes covered by these neocentromeres maintained wild-type expression levels. In contrast to *cen9*Δ mutants, *cen10*Δ mutant strains exhibited growth defects and were aneuploid for chromosome 10. At an elevated growth temperature (37°C), the *cen10*Δ chromosome was found to have undergone fusion with another native chromosome in some isolates and this fusion restored wild-type growth. Following chromosomal fusion, the neocentromere was inactivated, and the native centromere of the fused chromosome served as the active centromere. The neocentromere formation and chromosomal fusion events observed in this study in *C. deuterogattii* may be similar to events that triggered genomic changes within the *Cryptococcus*/*Kwoniella* species complex and may contribute to speciation throughout the eukaryotic domain.

Introduction

Eukaryotic organisms have linear chromosomes with specialized regions: telomeres that cap the ends, origins of replication, and centromeres that are critical for chromosome segregation. During cell division, the centromere binds to a specialized protein complex known as the kinetochore (Cheeseman, 2014). Most centromeres are regional, sequence-independent, and defined by the replacement of the canonical histone H3 by the histone homolog CENP-A (CenH3 or Cse4) (Henikoff and Furuyama, 2010). In humans, centromeres contain higher-order α-satellite DNA arrays that span 0.1 to 4.8 Mb (McNulty and Sullivan, 2018), which is in contrast to most fungal centromeres, which contain transposable elements and repetitive sequences (Friedman and Freitag, 2017). Fungal regional centromeres range from the small centromeres of *Candida albicans*, (the CENP-A enriched regions range from 2 to 3.3 kb and are located in 4 to 18 kb open-reading frame ORF-free regions), to the large regional centromeres described in *Neurospora crassa*, (which range from 174 to 287 kb and consist mainly of truncated transposable elements) (Sanyal et al., 2004; Smith et al., 2011). Similar to mice, some fungi have pericentric regions (Guenatri et al., 2004). The most prominent examples are the centromeres of *Schizosaccharomyces pombe,* which have a CENP-A-enriched region comprised of a central core flanked by heterochromatic pericentric regions divided into outer and inner repeats (Ishii et al., 2008; Rhind et al., 2011). Budding yeast have sequence-dependent centromeres, which are short and have a conserved organization with three centromere DNA elements (consensus DNA elements (CDEs) I-III) (Kobayashi et al., 2015). However, the budding yeast *Naumovozyma castellii* has unique consensus DNA elements that differ from those of other budding yeast species (Kobayashi et al., 2015).

Infrequently, centromeres can be spontaneously inactivated, resulting in neocentromere formation (i.e., evolutionarily new centromeres) (Ventura et al., 2007). Neocentromere formation can occur either while the native centromeric sequence is still present on the chromosome or when the native centromere has been mutated or deleted (e.g., from chromosomal rearrangements or γ irradiation damage (Burrack and Berman, 2012; Tolomeo et al., 2017; Ventura et al., 2007)). In addition, several studies have

described neocentromere formation after deletion of native centromeres by molecular genetic engineering in fungi, chickens, and *Drosophila* (Alkan et al., 2007; Ishii et al., 2008; Ketel et al., 2009; Shang et al., 2013). In some organisms, the formation of neocentromeres can be deleterious, leading to disease, cancer, or infertility (Burrack and Berman, 2012; Garsed et al., 2014; Nergadze et al., 2018; Scott and Sullivan, 2013; Warburton, 2004). For example, human neocentromeres are often identified in liposarcomas (Garsed et al., 2014). However, neocentromere formation also can be beneficial, leading to speciation (Ventura et al., 2007).

Fungal neocentromeres are well described in the diploid yeast *C. albicans* and the haploid fission yeast *S. pombe* (Ishii et al., 2008; Ketel et al., 2009; Thakur and Sanyal, 2013). Deletion of *C. albicans* native centromere 5 or 7 has been shown to induce neocentromere formation and does not result in chromosome loss (Ketel et al., 2009; Thakur and Sanyal, 2013). In these cases, neocentromeres conferred chromosomal stability similar to the native centromere (Ketel et al., 2009; Mishra et al., 2007). Deletion of a native centromere in *S. pombe* led to either neocentromere formation or chromosome fusion (Ishii et al., 2008; Ohno et al., 2016). *S. pombe* neocentromeres formed in telomere-proximal regions near heterochromatin, and neocentromere organization featured a CENP-A-enriched core domain and heterochromatin at the subtelomeric (distal) side. Interestingly, neocentromere formation occurred at the same regions in both wild-type and heterochromatin-deficient strains, suggesting that heterochromatin is dispensable for neocentromere formation in *S. pombe*, although the rate of survival by chromosome fusion was significantly increased in heterochromatin-deficient mutants (Ishii et al., 2008). Deletion of kinetochore proteins (*mhf1*Δ and *mhf2*Δ) led to a shift of CENP-A binding, resulting in a CENP-A-enriched region directly adjacent to the native centromere (Lu and He, 2019).

In some cases, neocentromeres span genes that are silenced, such as the neocentromeres in *C. albicans*. However the mechanisms that mediate silencing of neocentromeric genes are unknown in *C. albicans,* as proteins that are necessary for heterochromatin formation and gene silencing in other species (HP1, Clr4, and DNA

methyltransferase) are absent in *C. albicans* (Ketel et al., 2009). Neocentromeres of *S. pombe* can also span genes. These genes are upregulated during nitrogen starvation and expressed at low levels during stationary growth in wild-type cells, but are silenced under all conditions tested when spanned by neocentromeres. In addition to neocentromeric genes, genes located within native centromeres have been identified in other fungi as well as rice and chicken (Nagaki et al., 2004; Schotanus et al., 2015; Shang et al., 2013).

Recently, the centromeres of the human pathogenic fungus *Cryptococcus deuterogattii* were characterized and compared to those of the closely related species *Cryptococcus neoformans* (centromeres ranging from 27 to 64 kb), revealing dramatically smaller centromeres in *C. deuterogattii* (ranging from 8.7 to 21 kb) (Janbon et al., 2014; Yadav et al., 2018). *C. deuterogattii* is responsible for an ongoing outbreak in the Pacific Northwest regions of Canada and the United States (Fraser et al., 2005). In contrast to the sister species *C. neoformans*, *C. deuterogattii* commonly infects immunocompetent patients (Fraser et al., 2005). *C. deuterogattii* is a haploid basidiomycetous fungus with 14 chromosomes (D'Souza et al., 2011; Farrer et al., 2015; Yadav et al., 2018). The dramatic reduction in centromere size in *C. deuterogattii* may be attributable to loss of the RNAi pathway (Farrer et al., 2015; Yadav et al., 2018). The centromeres of *C. deuterogattii* consist of truncated transposable elements, and active transposable elements are missing throughout the genome (Yadav et al., 2018). This is in stark contrast to *C. neoformans,* which has active transposable elements in centromeric regions (Dumesic et al., 2015; Janbon et al., 2014; Yadav et al., 2018).

Neocentromeres are frequently formed near genomic repeats, yet *C. deuterogattii* lacks active transposons that might seed neocentromere formation. Thus, *C. deuterogattii* is a unique organism in which to study centromere structure and function. To elucidate centromeric organization, the native centromeres of chromosomes 10 and 9 were deleted, leading to characterization of the first neocentromeres in the *Basidiomycota* phylum of the fungal kingdom.

Materials and methods

Strains, primers, and culture conditions

Primers are listed in Supplementary Table S1. Strains used in this study are listed in Supplementary Table S2. All strains were stored in glycerol at -80°C, inoculated on solid YPD (yeast extract, peptone, and dextrose) media, and grown for two days at 30°C. Liquid YPD cultures were inoculated from single colonies of solid media and grown, while shaking, at 30°C overnight.

Genetic manipulations

DNA sequences (1 to 1.5 kb) of the *CEN10*-flanking regions were PCR-amplified with Phusion High-Fidelity DNA Polymerase (NEB, Ipswich MA, USA). Flanking regions were fused on both sides of either the *NEO* or *NAT* dominant selectable marker via overlap PCR, conferring G418 or nourseothricin resistance, respectively. Deletion of *C. deuterogattii CEN10* was achieved through homologous recombination via biolistic introduction of an overlap-PCR product as previously described (Billmyre et al., 2017; Davidson et al., 2002). Deletion of *CEN9* was performed by CRISPR-CAS9 mediated transformation with two guide RNAs flanking *CEN9* and homologous recombination was mediated by the introduction of an overlap PCR product as previously described (Fan and Lin, 2018). Transformants were selected on YPD medium containing G418 (200 μg/mL) or nourseothricin (100 μg/mL)

Subsequently, the 5' junction, 3' junction, and spanning PCR and Southern blot analyses were performed to confirm the correct replacement of *CEN10* by the appropriate drug resistance marker. To identify centromeres, the gene CNBG_0491, which encodes CENP-A, was N-terminally fused to the gene encoding the fluorescent mCherry protein by overlap PCR, and *C. deuterogattii* strains were biolistically transformed as previously described (Billmyre et al., 2017). A subset of *cen9*Δ mutants were biolistically transformed with an overlap PCR product containing *CENPC* C-terminally fused with *GFP*. As three *cen10*Δ mutants have a neocentromere that spans the gene encoding CENPC, a subset of *cen10*Δ mutants were transformed instead with an overlap PCR product containing *MIS12* C-terminally fused with *GFP*. Both PCR products encoding *CENPC-GFP* and *MIS12-GFP* were

randomly integrated in the genome and confirmed by a PCR spanning either *CENPC-GFP* or *MIS12-GFP*.

Growth and competition assays

Three replicate cultures for seven independent *cen10*Δ deletion mutants and the wild-type strain were grown in liquid YPD at 30°C overnight. Cells were diluted to an OD_{600} of 0.01 and grown in 50 mL YPD at 30°C. The OD_{600} of the triplicate cultures was measured every two hours with a SmartSpec 3000 (BioRad) until stationary phase was reached (T = 22 h).

For competition assays, three independent replicate cultures (*cen9*Δ, *cen10*Δ, control, and wild type) were grown overnight in 8 mL YPD. Subsequently, the cell density of the cultures was determined using a hemocytometer. For each independent *cen*Δ deletion mutant, 500,000 cells were co-cultured in a 1:1 ratio with wild-type cells. After 24 hours, the cultures were inoculated on 1) a YPD plate to determine the total colony-forming units (CFUs) and 2) a YPD plate containing G418 or nourseothricin to calculate the proportion of *cen10*Δ mutant CFUs compared to the wild-type CFUs. Plates were incubated at 30°C and the colonies were counted after 4 days. The cell morphology of >1000 cells of the wild type and of five *cen10*Δ mutant strains was analyzed, and the number of elongated cells was quantified (Figure S9).

Whole-genome sequencing, read mapping for aneuploidy/RNA-seq, and *de novo* genome assemblies

Genomic DNA was isolated using the CTAB protocol and sent to the Duke University Sequencing and Genomic Technologies Shared Resource facility for library preparation and Illumina sequencing. Sequencing was performed with a HiSeq 4000 sequencer, and 150 bp paired-end reads were generated. The resulting DNA sequence reads were trimmed, quality-filtered, and subsequently mapped with Bowtie2 to a complete PacBio, Nanopore-based, Illumina Pilon-corrected, whole-genome assembly of the *C. deuterogattii* R265 reference genome (version R265_fin_nuclear). Reads were visualized with IGV (Langmead,

2010; Quinlan and Hall, 2010; Thorvaldsdóttir et al., 2013; Yadav et al., 2018). Previously generated RNA sequencing reads (NCBI, SRA: SRR5209627) were remapped to the *C. deuterogattii* R265 reference genome by HISAT2 according to the default settings (de Oliveira Schneider et al., 2012; Pertea et al., 2016).

Genomes were *de novo* assembled with Spades using the default conditions (Bankevich et al., 2012). Genome assemblies were confirmed with PCRs using primers flanking the chromosome fusions and the PCR products obtained span the chromosomal fusions (Figure S7). The read coverage at chromosome fusions was analyzed and compared to the average read coverage of the contig (Figure S7).

Chromatin immunoprecipitation (ChIP) followed by high-throughput sequencing or qPCR

ChIP analyses were performed as previously described with minor modifications (Schotanus et al., 2015; Soyer et al., 2015). In short, 500 mL YPD cultures (1000 ml YPD for Mis12 ChIPs) were grown overnight at 30^{o}C, after which 37% formaldehyde was added to a final concentration of 0.5% for crosslinking. The cultures were then incubated for 15 minutes, formaldehyde was quenched with 2.5 M glycine (1/20 volume), and cells were washed with cold PBS. The crosslinking time of Mis12-GFP tagged isolates was extended to 45 minutes. Cells were resuspended in chromatin buffer (50 mM HEPES-NaOH, pH 7.5; 20 mM NaCl; 1 mM Na-EDTA, pH 8.0; 1% [v/v] Triton X-100; 0.1% [w/v] sodium deoxycholate [DOC]) containing protease inhibitors (cOmplet™ Tablets, mini EDTA-free EASYpack, Roche), followed by homogenization by bead beating with a miniBead beater (BioSpec products) using 18 cycles of 1.5 min on and 1.5 min off. The supernatant containing chromatin was sheared by sonication (24 cycles of 15 sec on, 15 sec off, burst at high level) (Bioruptor UCD-200, Diagenode). Chromatin was isolated by centrifugation, and the supernatant was divided into a sample fraction and a sonication control. The sample fraction was precleared with protein-A beads (1 to 3 hrs) and subsequently divided into two aliquots. One tube served as the input control, and a mCherry antibody (ab183628, Abcam) was added to the remaining half of the sample. The samples were incubated overnight at 4^{o}C and then processed according to a previously published

protocol (Soyer et al., 2015). After completing the ChIP experiment, the samples were analyzed by ChIP-qPCR or sent to the Duke University Sequencing and Genomic Technologies Shared Resource facility for library preparation and Illumina sequencing. Samples *cen10*Δ-A, *cen10*Δ-B and *cen10*Δ-C were sequenced with a HiSeq 2500 sequencer, and single reads of 50 bp were obtained. All other ChIP-seq samples were sequenced with a NovaSeq 600 sequencer and 50 bp PE reads were obtained. For each centromere mutant and the wild type, a ChIPed and input sample were sequenced. Reads were mapped to the reference genome, similar to the whole-genome sequencing reads. To analyze the ChIP-seq data the ChIPed sample was normalized with the input sample and visualized with the IGV viewer.

RNA isolation and qPCRs

Cells were grown in an overnight culture of 25 mL YPD at 30^{o}C. RNA was isolated with TRIzol™ LS (Thermo Fisher Scientific) according to the manufacturer's instructions. Subsequently, cDNA was synthesized with the SuperScript™First-Strand Synthesis System (Thermo Fisher Scientific) according to the manufacturer's instructions. qPCRs were performed in triplicate with Brilliant III Ultra-Fast SYBR® Green qPCR Master Mix (Agilent Technologies) on an ABI 1900HT qPCR machine.

Pulsed-field gel electrophoresis (PFGE)

Isolation of whole chromosomes and conditions for PFGE and chromoblot analysis were performed as previously described (Findley et al., 2012).

Deposited data

ChIP and whole-genome sequencing reads and *de novo* genome assemblies were deposited under NCBI BioProject Accession ID: #####.

Results

Deletion of centromere 9 and 10 results in neocentromere formation

To determine if neocentromere formation occurs in the *C. deuterogattii* reference strain R265, either centromere 9 or 10 was deleted. Biolistic transformation was used to replace centromere 10 (*CEN10*) with either the *NAT* or *NEO* dominant drug-resistance gene via homologous recombination. Centromere 9 (*CEN9*) was deleted by CRISPR-Cas9-mediated transformation. Two guide RNAs flanking the centromere were used and *CEN9* was replaced with a *NAT* dominant drug-resistance gene by homologous recombination. Viable transformants with the correct integration and deletion were obtained and confirmed by 5' junction, 3' junction, loss of deleted regions, and spanning PCRs as well as Southern blot analysis for *cen10*Δ (Figure S1, S2). Multiple independent *cen9*Δ and *cen10*Δ deletion mutants (*cen9*Δ-A to -F and *cen10*Δ-A to -G) were obtained from independent transformations. Pulsed-field gel electrophoresis (PFGE) confirmed that *cen*Δ mutants had a wild-type karyotype and that chromosome 9 and 10 remained linear, because a circular chromosome would not have entered the gel (Figure S3).

The formation of neocentromeres in *C. deuterogattii* was infrequent. A total of 99 independent biolistic transformations resulted in only seven confirmed *cen10*Δ mutants (7/21 total candidate transformants, 33% homologous integration), suggesting that *CEN10* deletion is lethal in most circumstances. In comparison, deletion of nonessential genes by homologous recombination in the *C. deuterogattii* R265 strain typically results in ~100 colonies with a high success rate (~80-90% homologous integration). We estimate that the likelihood of deleting a centromere and recovering a viable colony is at least 1000-fold lower than would be expected from the deletion of a non-essential gene. The deletion of *CEN9* was more efficient as this was mediated by CRISPR-Cas9 cleavage with two guide RNAs and a repair allele.

Chromatin immunoprecipitation of mCherry-CENP-A followed by high-throughput sequencing (ChIP-seq) for six *cen9Δ* (-A to -F) and seven *cen10*Δ mutants (-A to -G) was performed. Prior to the ChIP-seq experiment, all of the centromere deletion mutants were streak purified from single colonies. The sequence reads were mapped to a complete

whole-genome assembly, followed by the normalization of the reads by subtraction of the input from the ChIPed sample (Yadav et al., 2018). To quantify the ChIP-seq data, the CENP-A-enriched regions were compared with the centromeres previously identified based on CENPC enrichment. Both the CENP-A- and CENPC-enriched peaks were congruent for all of the native centromeres (Yadav et al., 2018). This analysis identified 13 of the 14 native centromeres (*CEN1-8*, *CEN11-14* and depending on the centromere mutant either *CEN9* or *CEN10*), indicating that, as expected, the native centromere of chromosome 9 or 10 was missing in all of the *cen9*Δ and *cen10*Δ deletion mutants respectively (Figure 1). Instead, neocentromeres were observed.

Except for the neocentromere of isolate *cen10*Δ-E, the neocentromeres formed in close proximity to the native centromere (*CEN9* and *CEN10*). Almost all neocentromeres were shorter than the native centromere, with the exception of *cen10*Δ-G which was larger than native centromere 10.

In three of the independent *cen9*Δ mutants (*cen9*Δ-B, -C and -E), neocentromeres formed at the same chromosomal location. Interestingly, two independent *cen10*Δ mutants (*cen10*Δ-A and *cen10*Δ-C) contained two CENP-A-enriched regions on chromosome 10, with a primary peak and a smaller secondary peak with reduced levels of CENP-A (1.3- to 1.75-fold lower) compared to the primary CENP-A peak. The chromosomal location of the secondary peak was similar to the neocentromere of *cen10*Δ-B (which had only one neocentromere).

The two CENP-A-enriched regions suggest four possible models: 1) aneuploidy in which cells harbor two chromosomes, 2) a dicentric chromosome with two neocentromeres (neodicentric), 3) instability between two different neocentromere states (neocentromere switching), 4) or only one CENP-A-enriched region functions as a centromere and the second CENP-A-enriched region is not bound by the kinetochore (Figure 1).

The neocentromeres were located in unique, nonrepetitive sequences and were not flanked by repetitive regions. The GC content of neocentromeres is similar to the overall GC content of chromosome 9 and 10, whereas the native centromere has a lower

GC content (Table 1). Comparing the reference genome with *de novo* genome assemblies of *cen10*Δ-A, *cen10*Δ-B, and *cen10*Δ-E confirmed that transposable elements did not enter these genomic regions during neocentromere formation (Table S4). Instead of spanning repeats and transposable elements like the native centromeres, neocentromeres span genes. The majority of the genes (24/28) flanking native centromeres are transcribed in the direction towards the native centromere. All of the neocentromeres observed span one or more genes and most of the flanking genes are transcribed in the direction away from the neocentromere.

Several of the genes spanned by neocentromeres are hypothetical genes, and interestingly, the kinetochore protein CENPC was located inside the neocentromere of *cen10*Δ-B and in the secondary peak of *cen10*Δ-A and -C (Table 1). The neocentromere in *cen10*Δ-B spanned 4.46 kb, was located 242 kb away from the 3' region of the native *CEN10*, and was located 115 kb from the telomere. In addition to the gene encoding CENPC, the CENP-A-enriched region spanned a hypothetical protein (Table 1). The primary CENP-A-enriched region of *cen10*Δ-A and *cen10*Δ-C spanned a gene encoding a serine/threonine-protein phosphatase 2A activator 2 (RRD2) and a hypothetical protein. This neocentromere spanned 2.85 kb and was located closer to the native *CEN10* (21 kb from the native centromere) than the neocentromere of *cen10*Δ-B and the secondary CENP-A peak of *cen10*Δ-A and *cen10*Δ-C. The neocentromere of *cen10*Δ-D was the smallest neocentromere (2.5 kb) and partially (88.4%) spanned a gene encoding a Ser/Thr protein kinase and formed 7.4 kb from the location of the native *CEN10*. The neocentromere of *cen10*Δ-E spanned two hypothetical proteins, was 4.38 kb in length and was located directly adjacent to the right telomere. Mutant *cen10*Δ-F had a neocentromere of 2.64 kb, which spanned one hypothetical gene completely and two genes (hypothetical and a hexokinase (*HXK1*)) partially; the neocentromere formed at a chromosomal location 20 kb 5' of the native centromere. The neocentromere of *cen10*Δ-G was the largest neocentromere with a CENP-A-enriched region of 7.97 kb, and was in fact larger than the native *CEN10*. This neocentromere spanned four genes, including a

gene coding for a high osmolarity protein (Sho1) and three genes coding for hypothetical proteins.

Like the neocentromeres of *cen10*Δ mutants, the neocentromeres of *cen9*Δ mutants also spanned genes. All of the neocentromeres formed in a region within 26 kb of the chromosomal location of the native centromere 9. Interestingly, the neocentromeres of *cen9*Δ-B, *cen9*Δ-C and *cen9*Δ-E all formed at the same chromosomal location and had the same length (4.41 kb); these neocentromeres spanned three genes. One gene was completely covered by CENP-A and this gene encoded a transglycosylase SLT domain-containing protein. The two other genes (a gene encoding a xylosylphosphotransferase and a gene encoding glutamate synthase (NADPH/NADH)) were partially covered with CENP-A. Mutant *cen9*Δ-A had a 3.87-kb long neocentromere located 26 kb 3' to the native centromere and spanned two genes. The first gene was completely spanned by CENP-A and encoded an ESCRT-II complex subunit (Vps25) protein. The second gene was only partially covered and encoded an iron regulator 1 protein. The neocentromere of *cen9*Δ-D was located directly to the left of the native centromere and was 4.37 kb in length. This neocentromere spanned two genes, coding for a hypothetical protein (92% covered by CENP-A) and a gene encoding for Derlin-2/3 that was completely covered by CENP-A. Lastly, the neocentromere of mutant *cen9*Δ-F was 3.83 kb in length and spanned one gene (encoding a xylosylphosphotransferase, Xpt1), which was completely covered by CENP-A. This neocentromere was located 12 kb away (3') from the native centromere 9.

To test if the kinetochore was binding to the CENP-A-enriched regions of chromosomes 9 and 10, and to validate if the neocentromeres were fully functional as centromeres, two additional kinetochore proteins were epitope-tagged with GFP. As the neocentromeres of three *cen10*Δ mutants spanned the gene encoding CENP-C, all *cen10*Δ mutants were transformed with an overlap PCR product, expressing Mis12-GFP. *cen9*Δ mutants were transformed with an overlap PCR product expressing CENPC-GFP. In addition to the *cen9*Δ and *cen10*Δ mutants, the wild type was transformed with constructs expressing Mis12-GFP and CENP-C-GFP, and these served as controls. ChIP-qPCRs for

*cen9*Δ mutants, *cen10*Δ mutants, and wild-type strains with Mis12-GFP or CENP-C-GFP were performed. Because Mis12 is an outer kinetochore protein, the formaldehyde cross-linking was extended to 45 minutes (15 minutes was used for CENP-A and CENP-C) for this protein. For all qPCR analyses, the native centromere 6 was used as an internal control and for each neocentromere specific primer pairs were designed. For *cen9*Δ and *cen10*Δ mutants a similar level of Mis12 or CENP-C enrichment at the neocentromeres and native centromere 6 was observed. This suggested that the CENP-A-enriched regions of chromosome 9 of the *cen9*Δ mutants and chromosome 10 of *cen10*Δ mutants identified by ChIP-seq were functional centromeres and indeed neocentromeres (Figure S4).

Previously generated RNA sequence data was remapped to the *C. deuterogattii* reference strain R265 and analyzed to determine if the regions where neocentromeres formed in the *cen*Δ mutants were transcribed in the wild type (Figure 1)(Table S3) (de Oliveira Schneider et al., 2012). In the wild-type strain, all genes spanned by neocentromeres in the *cen*Δ mutants were expressed. The expression levels of the neocentromeric genes in *cen9*Δ and *cen10*Δ mutants were assayed by qPCR. The neocentromeric genes of chromosome 9 were normalized to actin. To compensate for the ploidy levels of chromosome 10 in *cen10*Δ mutants, a housekeeping gene located on chromosome 10 was used to normalize the expression of genes spanned by neocentromeres located on chromosome 10. The expression levels of the CENP-A-associated neocentromeric genes were all found to be similar to the wild-type strain (Figure 2).

Neocentromere formation can reduce fitness

*cen10*Δ mutants were noted to grow more slowly than wild type. To investigate this, the growth of *cen10*Δ and wild-type strains was measured during the course of a 22-hour cell growth experiment. The majority of *cen10*Δ mutants exhibited slower growth rates compared to the wild-type parental strain R265. Six of seven *cen10*Δ mutants exhibited significant fitness defects compared to the wild-type strain, with doubling times ranging from 101 to 111 minutes compared to 81 minutes for the wild type (Figure 3). In

contrast, one mutant (*cen10*Δ-E) grew similarly to the wild type and had a similar doubling time (84 min for the mutant vs 81 min for the wild-type strain). Compared to the wild type, *cen10*Δ mutants with increased doubling times produced smaller colonies during growth on non-selective media.

To compare fitness, a competition assay was performed with 1:1 mixtures of wild-type and *cen9*Δ or *cen10*Δ mutants grown in liquid YPD medium. With no growth defect, the expectation was that the wild-type strain and centromere deletion mutants would grow at the same growth rate, resulting in a 1:1 ratio. In fact, fewer *cen10*Δ cells were found in the population after growth in competition with the wild-type strain, and this observation is consistent with the slower doubling time of *cen10*Δ mutants resulting in reduced fitness compared to wild type (Figure 3). Compared to the wild-type cells, there were fewer *cen9*Δ mutant cells in the population. However, the number was closer to a 1:1 ratio. The ratio of the *cen9*Δ mutants in the population was similar to the ratio of the *cen10*Δ-E mutant, which had a wild-type growth rate. Due to this observation, we hypothesize that the growth rate of the *cen9*Δ mutants is similar to wild type.

_cen10_Δ isolates are aneuploid

Because deletion of a centromere could lead to defects in chromosome segregation, *cen*Δ mutants were assessed for aneuploidy (Figure 4). Overall, *cen10*Δ mutants exhibited a mixture of large and small colony sizes during growth on YPD medium at 37°C.

Aneuploidy in *C. neoformans* often leads to a similar mixed colony size phenotype as that observed in the *cen10*Δ mutants (Sun et al., 2014). To exacerbate the aneuploidy-associated slow growth phenotype, four *cen10*Δ mutants were grown at elevated temperature (37°C), causing these isolates to produce smaller, growth-impaired and larger, growth-improved colonies (Figure S5). Three small and two large colonies were selected from each isolate and whole-genome analysis was performed based on Illumina sequencing. Sequences were mapped to the reference R265 genome, revealing that the small colonies were indeed aneuploid (Figure 4A). The small colonies of *cen10*Δ-B and

*cen10*Δ-C had ploidy levels for chromosome 10 in the range of 1.25- to 1.36-fold higher compared to the other 13 chromosomes, which suggested that only a proportion of the cells (25 to 36%), were aneuploid. The remainder of the genome was euploid. Chromosome 10 of the small colonies derived from isolate *cen10*Δ-A and *cen10*Δ-E exhibited ploidy levels ranging from 1.1- to 1.14-fold, reflecting less aneuploidy. Importantly, for all of the large colonies derived from isolates *cen10*Δ-A, *cen10*Δ-B, *cen10*Δ-C, and *cen10*Δ-E the fold coverage of chromosome 10 was restored to the wild-type euploid level (1.0 fold compared to wild type). The ploidy levels of chromosome 10 were 1-fold for all of the large colonies compared to wild type, indicating that the ploidy level of chromosome 10 of the large colonies was restored to euploid.

_cen10_Δ chromosome is rescued by chromosome fusion

Based on whole-genome sequencing and PFGE analysis, fusion of *cen10*Δ chromosome 10 to other chromosomes was a common event in the large colonies. Whole-genome sequence analysis revealed that sequences corresponding to the 3' subtelomeric region of chromosome 10 (including 1 gene) were absent in the sequences obtained from all of the large colonies analyzed (Figure S6). In addition, the large colonies of *cen10*Δ-A were missing sequences for two genes in the 5' subtelomeric region of chromosome 4. Large colonies of *cen10*Δ-B were missing 18.5 kb at the 5' subtelomere of chromosome 7 (including eight genes). The large colonies of *cen10*Δ-E lacked a small part of one gene in the 3' subtelomeric region of chromosome 1. In total, of the 14 subtelomeric genes that were lost in these three chromosome-fusion isolates, ten encoded hypothetical proteins and four encoded proteins with predicted functions. Seven genes have homologs in *C. neoformans* and are present in *C. neoformans* deletion libraries (Table S5). This observation suggested that either subtelomeric deletions occurred, or that chromosomal fusions led to the loss of subtelomeric regions. Notably, sequences from the small colonies spanned the entire genome with no evidence of these subtelomeric deletions (Figure S6).

We hypothesized that the subtelomeric gene loss was due to chromosomal fusion and tested this hypothesis with *de novo* genome assemblies and PFGE (Figure 5 and Figure

6). Based on *de novo* genome assemblies for the large colonies of *cen10*Δ-A, *cen10*Δ-B, and *cen10*Δ-E, chromosome 10 fused with chromosome 4, 7, or 1, respectively (Figure 5 and Table S5). In the large colony of *cen10*Δ-A (*cen10*Δ-A-L), the fusion occurred between chromosome 10 and chromosome 4. Chromosomal fusion led to the loss of the CNBG_10211 gene (on chromosome 4), and the fusion junction was within the CNBG_6174 gene of chromosome 4. For *cen10*Δ-B-L, the chromosomal fusion occurred between chromosomes 10 and 7. Seven genes of chromosome 7 were lost in the fused chromosome. The chromosome fusion junction was intergenic on chromosome 7. *cen10*Δ-E-L was due to a chromosomal fusion between chromosomes 10 and 1. The fusion was intragenic for both chromosomes. The fusion point occurred in CNBG_6141 on chromosome 10 and CNBG_10308 on chromosome 1.

Because all of the large *cen10*Δ colonies had chromosome 10 fusions, we examined the fusion location on chromosome 10 in detail. The fusions occurred 1.7, 0.3, and 3.6 kb from the chromosome 10 gene CNBG_6142, respectively (Figure 5 and S8). The fusion occurred in unique DNA sequences and was not flanked by repetitive regions. The overlapping region between chromosome 10 and the fused chromosome was at most 6 bp, suggesting that these fusions occurred via microhomology-mediated end joining (MMEJ) (also known as alternative nonhomologous end-joining [Alt-NHEJ]).

Chromosome fusion may result in loss of the neocentromeres, and the kinetochore may bind to the native centromere of the fused chromosome and function as the active centromere. This hypothesis was tested by performing ChIP-qPCR for CENP-A binding (Figure 6). For each neocentromere (either of the *cen10*Δ-A or *cen10*Δ-B mutant), CENP-A enrichment was tested with four primer sets located in the neocentromere. The CENP-A enrichment for these four locations was tested in 1) the initial *cen10*Δ mutant 2) a large colony derived from a specific *cen10*Δ mutant and 3) wild type. As expected, the ChIP-qPCR analysis showed CENP-A enrichment for the neocentromeres of the initial *cen10*Δ-A and *cen10*Δ-B mutants. The neocentromeric regions of *cen10*Δ-A and *cen10*Δ-B were not enriched with CENP-A in the wild-type strain, showing there was no occupancy by CENP-A prior to neocentromere formation. For all analyzed *cen10*Δ chromosome 10 fusion

isolates, the neocentromeres were not CENP-A-associated, and were similar to the wild-type background levels. Therefore, the neocentromeres were no longer active in the chromosome fusion strains(Figure 6). This suggests that the native centromere of the fusion partner of chromosome 10 (i.e., chromosome 1, 4, or 7) was the active centromere of the Chr10-Chr1, Chr10-Chr4, and Chr10-Chr7 fusions.

In addition to *cen10*Δ-A, -B, and -E mutants, whole-genome sequencing was performed for two large colonies of *cen10*Δ-C. Although it was not possible to identify the chromosome fusion based on whole-genome sequencing data for either of the large colonies of the *cen10*Δ-C mutant, PFGE analysis showed that *cen10*Δ-C-L1 had a fusion between chromosomes 10 and 13 (Figure 6b).

*cen10*Δ-C-L2 had read coverage of 1.99-fold for a region of ~200 kb of chromosome 10 (Figure 4). The rest of chromosome 10 was euploid, suggesting that the ~200 kb region was duplicated and was either a single chromosome or fused to another chromosome in this isolate. PFGE analysis suggested that this fragment was duplicated on chromosome 10, resulting in a larger chromosome (Figure 6). In contrast to the other fused chromosomes, this chromosomal fragment did not fuse to a chromosome with a native centromere, and the fact that the mutant still exhibited a fitness defect was consistent with this interpretation. The larger chromosome was euploid, suggesting that the unstable neocentromere(s), rather than causing aneuploidy, resulted in a fitness cost in this isolate.

Discussion

Composition of neocentromeres in *C. deuterogattii*

The native centromeres of *C. deuterogattii* are found in repetitive regions and are flanked by, but do not contain, protein-encoding genes (Yadav et al., 2018). By contrast, neocentromeres of *C. deuterogattii* span genes, lack repetitive elements, and like the native centromeres, are flanked by genes. In general (with one exception), the neocentromeres of *C. deuterogattii* are significantly shorter than the native centromeres, whereas most neocentromeres in other species have similar lengths as the native centromeres.

Native centromeres of *S. pombe* have a central core that is enriched with CENP-A and flanked by repetitive pericentric regions (Ishii et al., 2008). While neocentromere formation in *S. pombe* favors repeats in the pericentric regions, neocentromere formation is possible without the repetitive pericentric regions (Ishii et al., 2008). The majority of the neocentromeres in *C. albicans* and chickens are formed close to native centromeres due to seeding of CENP-A that is located near the native centromere (the so-called CENP-A cloud) (Ketel et al., 2009; Shang et al., 2013). The neocentromeres of *C. deuterogattii* follow the same trend and the majority of the neocentromeres formed close to the location of the native centromere. Our results and the earlier reports discussed, suggest that the chromosomal location of the native centromere is the main determinant of neocentromere formation. One exception was the neocentromere of *cen10*Δ-E, which directly flanked the left telomere. Interestingly, this was the only *cen10*Δ mutant that had a growth rate similar to wild type.

Several *C. deuterogattii* neocentromeres formed in the same location and a similar trend has been observed in neocentromere formation in *C. albicans* (Ketel et al., 2009). Evolutionary new centromeres (ECNs) in the largest crucifer tribe Arabideae originated several times independently and are located in the same chromosomal location (Mandáková et al., 2020). Although *C. deuterogattii* neocentromeres have the same chromosomal location, there is no apparent consensus between the different regions occupied by different neocentromeres. Also, there is no similarity to neocentromere

formation in other eukaryotes. Our results suggest that neocentromeres form by different mechanisms that do not rely on nearby transposable elements/repeats to initiate *de novo* centromere assembly.

Neocentromeric genes are expressed

Neocentromeres induced in several species can span genes, resulting in silencing or reduced gene expression. For example, all genes within five independent neocentromeres in *C. albicans* that spanned nine genes were suppressed (Burrack et al., 2016). In *S. pombe,* neocentromeres span genes that are only expressed in response to nitrogen starvation in the wild-type strain, and neocentromere formation silences these genes during nitrogen starvation (Ishii et al., 2008). The native centromere 8 of rice contains an approximately 750-kb CENP-A-enriched region with four genes that are expressed in both leaf and root tissues of three closely related species (Fan et al., 2011; Nagaki et al., 2004). Neocentromeres of rice span genes that are expressed at similar levels as in the wild type (Zhang et al., 2013). Chicken neocentromeres have been induced on chromosome Z or 5 (Shang et al., 2013). Chromosome Z neocentromeres span eight genes, but in wild-type cells only *MAMDC2* is expressed during normal growth. The other seven genes were either not expressed at any detectable level in all tested developmental stages or were only expressed during early embryonic stages (Shang et al., 2013). When a neocentromere formed, expression of the MAMDC2-encoding gene was reduced 20- to 100-fold. Chromosome 5 of chickens is diploid, and neocentromeres on this chromosome span genes that are expressed. The hypothesis behind this phenomenon is that one allele functions as a centromere, while the other allele codes for the genes.

Here, we showed that the neocentromeres in *C. deuterogattii* span two to three genes and that these genes are expressed at levels similar to the wild-type strain. Because the *cen10*Δ mutants of *C. deuterogattii* were aneuploid, the expression of genes spanned by chromosome 10 neocentromeres was normalized to expression levels of a housekeeping gene located on chromosome 10. Due to this internal chromosome 10 normalization, the hypothesis that the genes in the neocentromeres of *C. deuterogattii* are

still expressed because only one allele functions as a neocentromere can be rejected. The genes spanned by neocentromeres of *cen9*Δ mutants are also expressed at wild-type levels. As the *cen9*Δ mutants have uniform, wild-type colony sizes, the ploidy levels of these mutants were not tested and we hypothesize that these mutants are haploid/euploid. Based on this, and the modestly increased ploidy levels of *cen10*Δ mutants, we hypothesize the expression of neocentromeric genes is not due to the presence of an additional chromosome 10 allele. The expression of genes enriched for CENP-A chromatin is similar to that of wild type, and if the allelic hypothesis were valid, the expectation would be a 60% reduction in expression levels.

Genes contained in regions in which *C. deuterogattii* neocentromeres formed in *cen*Δ mutants were actively expressed in the wild-type strain, and this is similar to human neocentromeres that can form in regions with or without gene expression (Alonso et al., 2010; Marshall et al., 2008). However, the expression levels of the neocentromeric genes was lower than their neighboring genes. For example, the gene expression level of the gene (CNBG_5685) flanking native centromere 9 is three times higher than the genes spanned by neocentromeres in *cen9*Δ mutants. The same trend was observed in the *cen10*Δ mutants. Here, the expression level of the gene (CNBG_4365) 3' flanking the neocentromere (primary CENP-A peak) of *cen10*Δ-A and *cen10*Δ-C was more than six times higher than the genes spanned by the neocentromere. Also, the neocentromere of *cen10*Δ-D is flanked by genes whose expression was either 16 or two times higher than the genes spanned by the neocentromere. This suggests that neocentromeres are formed in chromosomal regions with lower gene expression in *C. deuterogattii*. However, we have identified chromosomal regions that lack gene expression on chromosomes 9 and 10, although these regions were not close to the native centromere.

Of the *C. deuterogattii* genes spanned by the neocentromere region, one encodes the kinetochore component CENP-C. Several independent biolistic transformations were performed to delete the gene encoding CENP-C, but all attempts were unsuccessful. This suggests that *CENPC* is an essential gene and might explain why the gene is still expressed even when bound by CENP-A. In addition, introducing mCherry-CENP-C by homologous

recombination in the *cen10*Δ mutants was not successful, but tagging CENP-C in the wild-type strain and in the *cen9*Δ mutants was effective (Yadav et al., 2018). This suggests that the chromatin may be changed due to neocentromere formation.

In fission yeast, deletion of the gene encoding the CENP-C homolog *Cnp3* was lethal at 36°C, but mutants were still viable at 30°C (Suma et al., 2018). However, CENP-A was mislocalized in the *cnp3*Δ mutants. Another gene partially located inside a *C. deuterogattii* neocentromere encodes the serine/threonine-protein phosphatase 2A activator 2 (*RRD2*). The *RRD2* homolog is not essential in *S. cerevisiae* (Higgs and Peterson, 2005). The other three neocentromeric genes encode hypothetical proteins and are available as deletion mutants in *C. neoformans* gene deletion mutant libraries (Liu et al., 2008; Sun et al., 2014).

Compared with other haploid fungi, the neocentromeric genes of *C. deuterogattii* are similar to the native centromeric genes of the haploid plant pathogenic fungus *Zymoseptoria tritici*. *Z. tritici* has short regional centromeres with an average size of 10.3 kb, and 18 out of 21 native centromeres have a total of 39 expressed genes (Schotanus et al., 2015).

*cen10*Δ mutants with two CENP-A-enriched regions

In our study, two of the initial *cen10*Δ mutants had two CENP-A-enriched regions on chromosome 10, suggesting a putative dicentric chromosome. However, CENP-A was not equally distributed between the two CENP-A-enriched regions; one peak was more enriched for CENP-A (primary neocentromere) compared to the other (secondary neocentromere). The appearance of two CENP-A-enriched regions of *C. deuterogattii* *cen10*Δ mutants could be explained in a few ways. First, neocentromere formation could lead to a dicentric chromosome 10 in which the centromeres may differ in functional capacity. Dicentric chromosomes are not by definition unstable, for example the dominant-negative mutation of the mammalian telomere protein TRF2 results in chromosome fusions, leading to the formation of dicentric chromosomes (Stimpson et al., 2010). The formation of dicentric chromosomes occurred in 97% of the fused mammalian chromosomes, which were stable for at least 180 cell divisions (Stimpson et al., 2010).

Several microscopic studies showed that chromosomes with two regions of centromere-protein enrichment are stable (Higgins et al., 2005; Stimpson et al., 2012, 2010; Sullivan and Willard, 1998). This suggests that a dineocentric chromosome 10 could be stable in the population. Second, the two CENP-A-enriched peaks could be the result of a mixed population and either due to an unstable primary neocentromere and/or aneuploidy. The primary neocentromere could be associated with the majority of the cells, whereas the secondary CENP-A peak would be only found in a small number of cells (and the primary neocentromere is lost in these isolates). This is reflected by lower CENP-A enrichment for the secondary peak, and the hypothesis of putative dicentrics is due to a mixture of alleles in the population. Third, the neocentromeres could be unstable, which could lead to the formation of two CENP-A-enriched regions with centromere function switching between the regions. However, our data would argue against this latter model. Prior to the ChIP-seq analysis of the *cen10*Δ mutants, colonies were isolated by streak purification (eight times), suggesting that the presence of two distinct CENP-A peaks occurs continuously. Experimental evolution experiments, followed by ChIP-qPCR, could be conducted to test if the primary neocentromere becomes more stable over time. The independent *cen10*Δ-B mutant has only one neocentromere, and this neocentromere is located in the same region as the secondary CENP-A peak of *cen10*Δ-A and -C.

*cen10*Δ mutants are partially aneuploid

Neocentromere formation in chickens results in a low number of aneuploid cells (Shang et al., 2013). Based on whole-genome sequencing of a population of cells, the *C. deuterogattii cen10*Δ isolates are partially aneuploid for chromosome 10. For fully aneuploid isolates, the coverage of Illumina reads is expected to be 2-fold; the *cen10*Δ isolates with two CENP-A peaks showed aneuploidy levels up to 1.28-fold or were even euploid. This suggests that, like the chicken neocentromeric isolates, only a small number of cells in a population of *C. deuterogattii cen10*Δ isolates are aneuploid.

_cen10_Δ mutants have reduced fitness

In *C. albicans*, deletion of centromere 5 results in neocentromere formation, and these isolates have fitness similar to the wild-type strain (Ketel et al., 2009). Similar results were reported for neocentromeres in chicken and *S. pombe*, in which strains with neocentromeres or chromosome fusion have a growth rate similar to the wild-type strain (Ishii et al., 2008; Shang et al., 2013). *cen9*Δ mutants have a growth rate and uniform colony sizes similar to wild type. In contrast, *C. deuterogattii cen10*Δ mutants have reduced fitness, and competition assays showed that *cen10*Δ mutants were less fit compared to the wild-type strain. There was no correlation between reduced fitness and abnormal cell morphology.

The competition assays showed that both *cen9*Δ and *cen10*Δ mutants grow slower than the wild type. However, the fitness defects of *cen9*Δ strains are not as severe as the fitness defects of *cen10*Δ mutants. If centromere deletions occurred in nature, we hypothesize that the wild type would outcompete all of the *cen*Δ isolates. The virulence of the *cen*Δ mutants was not assayed. Based on reduced fitness of the *cen*Δ mutants we hypothesize that pathogenicity of the *cen*Δ mutants would be lower than the wild type. However, when chromosome fusion occurs the growth rate is restored to a near wild-type level and we hypothesize that the isolates with 13 chromosomes could have virulence similar to the wild type. Several genes were lost due to the fusion events in the *cen*Δ mutants; to our knowledge these lost genes have not been associated with pathogenicity of *C. deuterogattii.*

Neocentromere stains exhibit impaired growth and chromosome fusion restores wild-type growth at elevated temperatures

Deletion of a centromere in *S. pombe* leads to either neocentromere formation or chromosome fusion due to a noncanonical homologous recombination pathway (Ishii et al., 2008; Ohno et al., 2016). This is in contrast to neocentromere formation in *C. deuterogattii*, which results in 100% neocentromere formation. Based on PFGE analysis,

the karyotype of the *cen*Δ isolates is wild type at 30°C, but chromosome fusion can occur at 37°C within the *cen10*Δ mutants and lead to improved growth at 30°C.

The location of the *cen10*Δ neocentromere had no influence on the ability to undergo chromosome fusion. Chromosome fusions in three *cen10*Δ mutants were analyzed in more detail. Of these three *cen10*Δ mutants one *cen10*Δ mutant has two enriched CENP-A regions, with the primary peak close to the native centromere 10 (within 21 kb). The second *cen10*Δ mutant has a neocentromere located 118 kb away from the telomere and the third *cen10*Δ mutant has a telocentric neocentromere.

The fused chromosomes have no or only short homology at the breakpoints that is insufficient for homologous recombination, suggesting that the chromosome fusions arise via MMEJ. Future experiments to test this hypothesis could involve deleting genes involved in the MMEJ pathway, such as *CDC9* and *DNL4* (Sinha et al., 2016).

A prominent chromosome fusion occurred during the speciation of humans. Compared to other great apes, humans have a reduced karyotype, which is due to the fusion of two ancestral chromosomes that resulted in chromosome 2 in modern humans, Denisovans, and Neanderthals (Miga, 2017). Human chromosome 2 still harbors signatures of telomeric repeats at the fusion point (interstitial telomeric sequences [ITS]), suggesting that this chromosome is derived from a telomere-telomere fusion. By synteny analysis, the inactive centromere of chimpanzee chromosome 2b can be identified on human chromosome 2, and there are relics of α satellite DNA at this now extinct centromere (Miga, 2017). Moreover, a dominant-negative mutation of the human telomeric protein TRF2 leads to telomere-telomere fusions, mainly between acrocentric chromosomes (Stimpson et al., 2010; Van Steensel et al., 1998). In the fungal species *Malassezia,* chromosome breakage followed by chromosome fusion has led to speciation (Sankaranarayanan et al., 2020). The short regional centromeres (3-5 kb) are fragile and this led most likely to chromosome reduction. By contrast in *C. deuterogattii,* the chromosomes involved in chromosomal fusion of the *cen10*Δ mutants were all metacentric, and fusion occurred in nontelomeric sequences.

Another example of telomeric fusions is the presence of ITS regions in several genomes. In budding yeast, the experimental introduction of an ITS into an intron of the *URA3* gene resulted in four classes of chromosome rearrangements, including: 1) inversion, 2) gene conversion, 3) minichromosome formation due to deletion or duplication, and 4) minichromosome formation due to translocation (Aksenova et al., 2013). Based on our *de novo* genome assemblies of the *C. deuterogattii* large-colony *cen10*Δ mutants, chromosome fusions occurred with no signs of chromosome rearrangements. PFGE analysis of the initial *cen10*Δ mutants and the 37°C-derived large colonies showed that only chromosome 10 is fused to another chromosome and, except for the fused chromosome, all other chromosomes are wild type. BlastN analysis in the *de novo* genome assemblies of the large colonies confirmed that the subtelomeric regions, which were lost due to chromosomal fusion, were not located on minichromosomes or inserted in other chromosomes. Thus, these chromosome fusions did not produce ITS regions, which would otherwise destabilize the genome.

Conclusions

Our work shows that, like in other model systems, neocentromeres can be induced in *C. deuterogattii*. However, *C. deuterogattii* neocentromeres have several unique characteristics, such as spanning genes whose expression is unaffected by centromere assembly. In some instances, deletion of *CEN10* led to chromosome fusion, resulting in enhanced fitness and leading to inactivation of the neocentromere. Presumably, deletion of other centromeres could be carried out, leading to a *C. deuterogattii* strain with only one or a few chromosomes, as was recently reported in *S. cerevisiae* (Luo et al., 2018; Shao et al., 2018).

Acknowledgements

We thank Tom Petes, Beth Sullivan, Kaustuv Sanyal, Sue Jinks-Robertson, Vikas Yadav, Shelby Priest, Shelly Clancey, and Inge van der Kloet for comments on the manuscript. We would like to thank all of the members of the Heitman and Sanyal labs who contribute to the bi-weekly Skype meeting. These studies were supported by NIH/NIAID grants R01 AI050113-15 and R37 MERIT award AI039115-22 to JH. JH is co-director and fellow of the CIFAR program Fungal Kingdom: Threats & Opportunities.

Author contributions

Conceptualization: KS and JH. Formal analysis: KS. Investigation: KS. Resources: JH. Data curation: KS and JH. Writing - original draft: KS. Writing – review & editing: KS and JH. Visualization: KS. Supervision: JH. Project administration: KS and JH. Funding acquisition: JH.

Declaration of Interests

The authors declare no competing interests.

References

Aksenova AY, Greenwell PW, Dominska M, Shishkin AA, Kim JC, Petes TD, Mirkin SM. 2013. Genome rearrangements caused by interstitial telomeric sequences in yeast. *Proc Natl Acad Sci U S A* 1–6. doi:10.1073/pnas.1319313110

Alkan C, Ventura M, Archidiacono N, Rocchi M, Sahinalp SC, Eichler EE. 2007. Organization and evolution of primate centromeric DNA from whole-genome shotgun sequence data. *PLoS Comput Biol* **3**:e181. doi:10.1371/journal.pcbi.0030181

Alonso A, Hasson D, Cheung F, Warburton PE. 2010. A paucity of heterochromatin at functional human neocentromeres. *Epigenetics and Chromatin* **3**:6. doi:10.1186/1756-8935-3-6

Bankevich A, Nurk S, Antipov D, Gurevich AA, Dvorkin M, Kulikov AS, Lesin VM, Nikolenko SI, Pham S, Prjibelski AD, Pyshkin A V., Sirotkin A V., Vyahhi N, Tesler G, Alekseyev MA, Pevzner PA. 2012. SPAdes: A new genome assembly algorithm and its applications to single-cell sequencing. *J Comput Biol* **19**:455–477. doi:10.1089/cmb.2012.0021

Billmyre RB, Clancey SA, Heitman J. 2017. Natural mismatch repair mutations mediate phenotypic diversity and drug resistance in *Cryptococcus deuterogattii*. *eLife* **6**:e28802. doi:10.7554/eLife.28802

Burrack LS, Berman J. 2012. Neocentromeres and epigenetically inherited features of centromeres. *Chromosom Res* **20**:607–619. doi:10.1007/s10577-012-9296-x

Burrack LS, Hutton HF, Matter KJ, Clancey SA, Liachko I, Plemmons AE, Saha A, Power EA, Turman B, Thevandavakkam MA, Ay F, Dunham MJ, Berman J. 2016. Neocentromeres provide chromosome segregation accuracy and centromere clustering to multiple loci along a *Candida albicans* chromosome. *PLoS Genet* **12**:e1006317. doi:10.1371/journal.pgen.1006317

Cheeseman IM. 2014. The kinetochore. *Cold Spring Harb Perspect Biol* **6**:a015826. doi:10.1101/cshperspect.a015826

D'Souza CA, Kronstad JW, Taylor G, Warren R, Yuen M, Hu G, Jung WH, Sham A, Kidd SE, Tangen K, Lee N, Zeilmaker T, Sawkins J, McVicker G, Shah S, Gnerre S, Griggs A,

Zeng Q, Bartlett K, Li W, Wang X, Heitman J, Stajich JE, Fraser JA, Meyer W, Carter D, Schein J, Krzywinski M, Kwon-Chung KJ, Varma A, Wang J, Brunham R, Fyfe M, Ouellette BFF, Siddiqui A, Marra M, Jones S, Holt R, Birren BW, Galagan JE, Cuomo CA. 2011. Genome variation in Cryptococcus gattii, an emerging pathogen of immunocompetent hosts. *mBio* **2**:e00342-10. doi:10.1128/mBio.00342-10

Davidson RC, Blankenship JR, Kraus PR, De M, Berrios J, Hull CM, Souza CD, Wang P, Heitman J. 2002. A PCR-based strategy to generate integrative targeting alleles with large regions of homology. *Microbiology* **2**:2607–2615.

de Oliveira Schneider R, de Souza Süffert Fogaça N, Kmetzsch L, Schrank A, Vainstein MH, Staats CC. 2012. Zap1 regulates zinc homeostasis and modulates virulence in *Cryptococcus gattii*. *PLoS One* **7**:e43773. doi:10.1371/journal.pone.0043773

Dumesic PA, Homer CM, Moresco JJ, Pack LR, Shanle EK, Coyle SM, Strahl BD, Fujimori DG, Yates JR, Madhani HD. 2015. Product binding enforces the genomic specificity of a yeast polycomb repressive complex. *Cell* **160**:204–218. doi:10.1016/j.cell.2014.11.039

Fan C, Walling JG, Zhang J, Hirsch CD, Jiang J, Wing RA. 2011. Conservation and purifying selection of transcribed genes located in a rice centromere. *Plant Cell* **23**:2821–30. doi:10.1105/tpc.111.085605

Fan Y, Lin X. 2018. Multiple applications of a transient CRISPR-Cas9 coupled with electroporation (TRACE) system in the *Cryptococcus neoformans* species complex. *Genetics* **208**:1357–1372. doi:10.1534/genetics.117.300656

Farrer RA, Desjardins CA, Sakthikumar S, Gujja S, Saif S, Zeng Q, Chen Y, Voelz K, Heitman J, May RC, Fisher MC, Cuomo CA. 2015. Genome evolution and innovation across the four major lineages of *Cryptococcus gattii*. *mBio* **6**:e00868-15. doi:10.1128/mBio.00868-15

Findley K, Sun S, Fraser JA, Hsueh YP, Averette AF, Li W, Dietrich FS, Heitman J. 2012. Discovery of a modified tetrapolar sexual cycle in *Cryptococcus amylolentus* and the evolution of *MAT* in the *Cryptococcus* species complex. *PLoS Genet* **8**:e1002528. doi:10.1371/journal.pgen.1002528

Fraser JA, Giles SS, Wenink EC, Geunes-Boyer SG, Wright JR, Diezmann S, Allen A, Stajich JE, Dietrich FS, Perfect JR, Heitman J. 2005. Same-sex mating and the origin of the Vancouver Island *Cryptococcus gattii* outbreak. *Nature* **437**:1360–1364. doi:10.1038/nature04220

Friedman S, Freitag M. 2017. Centrochromatin of fungi In: Black BE, editor. Centromeres and Kinetochores. Cham, Switzerland: Springer International Publishing. pp. 85–109. doi:10.1016/S0092-8674(03)00115-6

Garsed DW, Marshall OJ, Corbin VDA, Hsu A, DiStefano L, Schröder J, Li J, Feng ZP, Kim BW, Kowarsky M, Lansdell B, Brookwell R, Myklebost O, Meza-Zepeda L, Holloway AJ, Pedeutour F, Choo KHA, Damore MA, Deans AJ, Papenfuss AT, Thomas DM. 2014. The architecture and evolution of cancer neochromosomes. *Cancer Cell* **26**:653–667. doi:10.1016/j.ccell.2014.09.010

Guenatri M, Bailly D, Maison C, Almouzni G. 2004. Mouse centric and pericentric satellite repeats form distinct functional heterochromatin. *J Cell Biol* **166**:493–505. doi:10.1083/jcb.200403109

Henikoff S, Furuyama T. 2010. Epigenetic inheritance of centromeres. *Cold Spring Harb Symp Quant Biol* **75**:51–60. doi:10.1101/sqb.2010.75.001

Higgins AW, Gustashaw KM, Willard HF. 2005. Engineered human dicentric chromosomes show centromere plasticity. *Chromosom Res* **13**:745–762. doi:10.1007/s10577-005-1009-2

Higgs HN, Peterson KJ. 2005. Phylogenetic analysis of the formin homology 2 domain. *Mol Biol Cell* **16**:1–13. doi:10.1091/mbc.E04

Ishii K, Ogiyama Y, Chikashige Y, Soejima S, Masuda F, Kakuma T, Hiraoka Y, Takahashi K. 2008. Heterochromatin integrity affects chromosome reorganization after centromere dysfunction. *Science* **321**:1088–91. doi:10.1126/science.1158699

Janbon G, Ormerod KL, Paulet D, Byrnes EJ, Yadav V, Chatterjee G, Mullapudi N, Hon C-C, Billmyre RB, Brunel F, Bahn Y-S, Chen W, Chen Y, Chow EWL, Coppée J-Y, Floyd-Averette A, Gaillardin C, Gerik KJ, Goldberg J, Gonzalez-Hilarion S, Gujja S, Hamlin JL, Hsueh Y-P, Ianiri G, Jones S, Kodira CD, Kozubowski L, Lam W, Marra M, Mesner LD,

Mieczkowski PA, Moyrand F, Nielsen K, Proux C, Rossignol T, Schein JE, Sun S, Wollschlaeger C, Wood IA, Zeng Q, Neuvéglise C, Newlon CS, Perfect JR, Lodge JK, Idnurm A, Stajich JE, Kronstad JW, Sanyal K, Heitman J, Fraser JA, Cuomo CA, Dietrich FS. 2014. Analysis of the genome and transcriptome of *Cryptococcus neoformans var. grubii* reveals complex RNA expression and microevolution leading to virulence attenuation. *PLoS Genet* **10**:e1004261. doi:10.1371/journal.pgen.1004261

Ketel C, Wang HSW, McClellan M, Bouchonville K, Selmecki A, Lahav T, Gerami-Nejad M, Berman J. 2009. Neocentromeres form efficiently at multiple possible loci in *Candida albicans*. *PLoS Genet* **5**:e1000400. doi:10.1371/journal.pgen.1000400

Kobayashi N, Suzuki Y, Schoenfeld LW, Müller CA, Nieduszynski C, Wolfe KH, Tanaka TU. 2015. Discovery of an unconventional centromere in budding yeast redefines evolution of point centromeres. *Curr Biol* **25**:2026–2033. doi:10.1016/j.cub.2015.06.023

Langmead B. 2010. Aligning short sequencing reads with Bowtie. *Curr Protoc Bioinforma* 11.7.1-11.7.14. doi:10.1002/0471250953.bi1107s32

Liu OW, Chun CD, Chow ED, Chen C, Madhani HD, Noble SM. 2008. Systematic genetic analysis of virulence in the human fungal pathogen *Cryptococcus neoformans*. *Cell* **135**:174–188. doi:10.1016/j.cell.2008.07.046

Lu M, He X. 2019. Centromere repositioning causes inversion of meiosis and generates a reproductive barrier. *Proc Natl Acad Sci U S A* **116**:21580–21591. doi:10.1073/pnas.1911745116

Luo J, Sun X, Cormack BP, Boeke JD. 2018. Karyotype engineering by chromosome fusion leads to reproductive isolation in yeast. *Nature* **560**:392–396. doi:10.1038/s41586-018-0374-x

Mandáková T, Hloušková P, Koch MA, Lysak MA. 2020. Genome evolution in Arabideae was marked by frequent centromere repositioning. *Plant Cell*. doi:10.1105/tpc.19.00557

Marshall OJ, Chueh AC, Wong LH, Choo KHA. 2008. Neocentromeres: new insights into centromere structure, disease development, and karyotype evolution. *Am J Hum*

Genet **82**:261–282. doi:10.1016/j.ajhg.2007.11.009

McNulty SM, Sullivan BA. 2018. Alpha satellite DNA biology: finding function in the recesses of the genome. *Chromosom Res* **26**:115–138. doi:10.1007/s10577-018-9582-3

Miga KH. 2017. Chromosome-specific centromere sequences provide an estimate of the ancestral chromosome 2 fusion event in hominin genomes. *J Hered* **108**:45–52. doi:10.1093/jhered/esw039

Mishra PK, Baum M, Carbon J. 2007. Centromere size and position in *Candida albicans* are evolutionarily conserved independent of DNA sequence heterogeneity. *Mol Genet Genomics* **278**:455–65. doi:10.1007/s00438-007-0263-8

Nagaki K, Cheng Z, Ouyang S, Talbert PB, Kim M, Jones KM, Henikoff S, Buell CR, Jiang J. 2004. Sequencing of a rice centromere uncovers active genes. *Nat Genet* **36**:138–45. doi:10.1038/ng1289

Nergadze SG, Piras FM, Gamba R, Corbo M, Cerutti F, McCarter JGW, Cappelletti E, Gozzo F, Harman RM, Antczak DF, Miller D, Scharfe M, Pavesi G, Raimondi E, Sullivan KF, Giulotto E. 2018. Birth, evolution, and transmission of satellite-free mammalian centromeric domains. *Genome Res* **28**:789–799. doi:10.1101/gr.231159.117

Ohno Y, Ogiyama Y, Kubota Y, Kubo T, Ishii K. 2016. Acentric chromosome ends are prone to fusion with functional chromosome ends through a homology-directed rearrangement. *Nucleic Acids Res* **44**:232–244. doi:10.1093/nar/gkv997

Pertea M, Kim D, Pertea GM, Leek JT, Salzberg SL. 2016. Transcript-level expression analysis of RNA-seq experiments with HISAT, StringTie and Ballgown. *Nat Protoc* **11**:1650–1667. doi:10.1038/nprot.2016.095

Quinlan AR, Hall IM. 2010. BEDTools: A flexible suite of utilities for comparing genomic features. *Bioinformatics* **26**:841–842. doi:10.1093/bioinformatics/btq033

Rhind N, Chen Z, Yassour M, Thompson DA, Haas BJ, Habib N, Wapinski I, Roy S, Lin MF, Heiman DI, Young SK, Furuya K, Guo Y, Pidoux A, Chen HM, Robbertse B, Goldberg JM, Aoki K, Bayne EH, Berlin AM, Desjardins CA, Dobbs E, Dukaj L, Fan L, FitzGerald MG, French C, Gujja S, Hansen K, Keifenheim D, Levin JZ, Mosher RA, Muller CA,

Pfiffner J, Priest M, Russ C, Smialowska A, Swoboda P, Sykes SM, Vaughn M, Vengrova S, Yoder R, Zeng Q, Allshire RC, Baulcombe DC, Birren BW, Brown W, Ekwall K, Kellis M, Leatherwood J, Levin H, Margalit H, Martienssen RA, Nieduszynski CA, Spatafora JW, Friedman N, Dalgaard JZ, Baumann P, Niki H, Regev A, Nusbaum C. 2011. Comparative functional genomics of the fission yeasts. *Science* **930**:930–936. doi:10.1126/science.1203357

Sankaranarayanan SR, Ianiri G, Coelho MA, Reza MH, Thimmappa BC, Ganguly P, Vadnala RN, Sun S, Siddharthan R, Tellgren-Roth C, Dawson TL, Heitman J, Sanyal K. 2020. Loss of centromere function drives karyotype evolution in closely related *Malassezia* species. *eLife* **9**. doi:10.7554/eLife.53944

Sanyal K, Baum M, Carbon J. 2004. Centromeric DNA sequences in the pathogenic yeast *Candida albicans* are all different and unique. *Proc Natl Acad Sci U S A* **101**:11374–9. doi:10.1073/pnas.0404318101

Schotanus K, Soyer JL, Connolly LR, Grandaubert J, Happel P, Smith KM, Freitag M, Stukenbrock EH. 2015. Histone modifications rather than the novel regional centromeres of *Zymoseptoria tritici* distinguish core and accessory chromosomes. *Epigenetics Chromatin* **8**:41. doi:10.1186/s13072-015-0033-5

Scott KC, Sullivan BA. 2013. Neocentromeres: a place for everything and everything in its place. *Trends Genet* **30**:66–74. doi:10.1016/j.tig.2013.11.003

Shang W-HH, Hori T, Martins NMCC, Toyoda A, Misu S, Monma N, Hiratani I, Maeshima K, Ikeo K, Fujiyama A, Kimura H, Earnshaw WC, Fukagawa T. 2013. Chromosome engineering allows the efficient isolation of vertebrate neocentromeres. *Dev Cell* **24**:635–648. doi:10.1016/j.devcel.2013.02.009

Shao Y, Lu N, Wu Z, Cai C, Wang S, Zhang LL, Zhou F, Xiao S, Liu L, Zeng X, Zheng H, Yang C, Zhao Z, Zhao G, Zhou JQ, Xue X, Qin Z. 2018. Creating a functional single-chromosome yeast. *Nature* **560**:331–335. doi:10.1038/s41586-018-0382-x

Sinha S, Villarreal D, Shim EY, Lee SE. 2016. Risky business: Microhomology-mediated end joining. *Mutat Res Mol Mech Mutagen* **788**:17–24. doi:10.1016/j.mrfmmm.2015.12.005

Smith KM, Phatale PA, Sullivan CM, Pomraning KR, Freitag M. 2011. Heterochromatin is required for normal distribution of *Neurospora crassa* CenH3. *Mol Cell Biol* **31**:2528–2542. doi:10.1128/MCB.01285-10

Soyer JL, Möller M, Schotanus K, Connolly LR, Galazka JM, Freitag M, Stukenbrock EH. 2015. Chromatin analyses of *Zymoseptoria tritici* : Methods for chromatin immunoprecipitation followed by high-throughput sequencing (ChIP-seq). *Fungal Genet Biol* **79**:63–70. doi:10.1016/j.fgb.2015.03.006

Stimpson KM, Matheny JE, Sullivan BA. 2012. Dicentric chromosomes: unique models to study centromere function and inactivation. *Chromosome Res* **20**:595–605. doi:10.1007/s10577-012-9302-3

Stimpson KM, Song IY, Jauch A, Holtgreve-Grez H, Hayden KE, Bridger JM, Sullivan BA. 2010. Telomere disruption results in non-random formation of de novo dicentric chromosomes involving acrocentric human chromosomes. *PLoS Genet* **6**:e1001061. doi:10.1371/journal.pgen.1001061

Sullivan BA, Willard HF. 1998. Stable dicentric X chromosomes with two functional centromeres. *Nat Genet* **20**:227–228. doi:10.1038/3024

Suma M, Kitagawa T, Nakase Y, Nakazawa N, Yanagida M, Matsumoto T. 2018. Fission yeast CENP-C (Cnp3) plays a role in restricting the site of CENP-A accumulation. *G3* **8**:2723–2733. doi:10.1534/g3.118.200486

Sun S, Billmyre RB, Mieczkowski PA, Heitman J. 2014. Unisexual reproduction drives meiotic recombination and phenotypic and karyotypic plasticity in *Cryptococcus neoformans*. *PLoS Genet* **10**:e1004849. doi:10.1371/journal.pgen.1004849

Thakur J, Sanyal K. 2013. Efficient neocentromere formation is suppressed by gene conversion to maintain centromere function at native physical chromosomal loci in *Candida albicans*. *Genome Res* 638–652. doi:10.1101/gr.141614.112

Thorvaldsdóttir H, Robinson JT, Mesirov JP. 2013. Integrative genomics viewer (IGV): high-performance genomics data visualization and exploration. *Brief Bioinform* **14**:178–192. doi:10.1093/bib/bbs017

Tolomeo D, Capozzi O, Stanyon RR, Archidiacono N, D'Addabbo P, Catacchio CR, Purgato

S, Perini G, Schempp W, Huddleston J, Malig M, Eichler EE, Rocchi M. 2017. Epigenetic origin of evolutionary novel centromeres. *Sci Rep* **7**:41980. doi:10.1038/srep41980

Van Steensel B, Smogorzewska A, De Lange T. 1998. TRF2 protects human telomeres from end-to-end fusions. *Cell* **92**:401–413. doi:10.1016/S0092-8674(00)80932-0

Ventura M, Antonacci F, Cardone MF, Stanyon R, D'Addabbo P, Cellamare A, Sprague LJ, Eichler EE, Archidiacono N, Rocchi M. 2007. Evolutionary formation of new centromeres in macaque. *Science* **316**:243–246. doi:10.1126/science.1140615

Warburton PE. 2004. Chromosomal dynamics of human neocentromere formation. *Chromosom Res* **12**:617–26. doi:10.1023/B:CHRO.0000036585.44138.4b

Yadav V, Sun S, Billmyre RB, Thimmappa BC, Shea T, Lintner R, Bakkeren G, Cuomo CA, Heitman J, Sanyal K. 2018. RNAi is a critical determinant of centromere evolution in closely related fungi. *Proc Natl Acad Sci* 201713725. doi:10.1073/pnas.1713725115

Zhang B, Lv Z, Pang J, Liu Y, Guo X, Fu S, Li J, Dong Q, Wu H-J, Gao Z, Wang X-J, Han F. 2013. Formation of a functional maize centromere after loss of centromeric sequences and gain of ectopic sequences. *Plant Cell* **25**:1979–1989. doi:10.1105/tpc.113.110015

Tables

Table 1. Genes located inside neocentromeres.

The chromosomal locations, sizes, and GC content (%) for the native centromere and *cen*Δ mutants are shown. For the neocentromeres, gene ID, predicted function, and the amount of CENP-A coverage are indicated.

Table 1. Genes located inside neocentromeres.

	Chr coor (bp)	Size (kb)	Size compared to native centromere (%)	GC%	Genes spanned by neocentromere	Gene ID	% covered by Neocentromere	Exons inside neocentromere
Native centromere 9	Chr9:755,771-762,621	6.84	-	43.6	-	-	-	-
*cen9*Δ-A	Chr9:785,352-789,247	3.87	56.6	46.1	Escrt-II complex subunit (VPS25)	CNBG_5690	100	
					Iron regulator 1	CNBG_9614	14.6	Last exon
*cen9*Δ-B	Chr9:775,164-780,756	4.41	64.5	46.6	Xylosylphosphotransferase	CNBG_5687	6.9	
					Transglycosylase SLT domain-containing protein	CNBG_9613	100	
					Glutamate synthase (NADPH/NADH)	CNBG_5689	33.7	
*cen9*Δ-C	Chr9:775,164-780,756	4.41	64.5	46.6	Xylosylphosphotransferase	CNBG_5687	6.9	
					Transglycosylase SLT domain-containing protein	CNBG_9613	100	
					Glutamate synthase (NADPH/NADH)	CNBG_5689	33.7	
*cen9*Δ-D	Chr9:750,902-755,294	4.37	63.9	41.9	Hypothetical protein	CNBG_5684	92.8	
					Derlin-2/3	CNBG_5685	100	
*cen9*Δ-E	Chr9:775,164-780,756	5.56	81.3	50	Xylosylphosphotransferase	CNBG_5687	6.9	
					Transglycosylase SLT domain-containing protein	CNBG_9613	100	Last exon
					Glutamate synthase (NADPH/NADH)	CNBG_5689	33.7	Last exon
*cen9*Δ-F	Chr9:771,614-775,469	3.83	56.0	51.5	Xylosylphosphotransferase (XPT1)	CNBG_5687	100	
Native centromere 10	Chr10:362,876-369,657	6.77	-	42.6	-	-	-	-
*cen10*Δ-A	Chr10:115,954-120,422	4.46	65.9	46.9	*CENPC/MIF2*	CNBG_4461	88.3	1, 2, 3, 4 (only 5th is outside)
					Hypothetical protein	CNBG_4462	100	
	Chr10:391,090-393,946	2.85	42.1	48.9	Serine/threonine-protein phosphatase 2A activator 2*(RRD2)*	CNBG_9459	10.6	Last exon (5th)
					Hypothetical protein	CNBG_4366	100	
					Hypothetical protein	CNBG_4365	23.4	Last exon (3th)
*cen10*Δ-B	Chr10:115,954-120,422	4.46	65.9	46.9	*CENPC/MIF2*	CNBG_4461	88.3	1, 2, 3, 4 (only 5th is outside)
					Hypothetical protein	CNBG_4462	100	
*cen10*Δ-C	Chr10:115,954-120,422	4.46	65.9	46.9	*CENPC/MIF2*	CNBG_4461	88.3	1, 2, 3, 4 (only 5th is outside)
					Hypothetical protein	CNBG_4462	100	
	Chr10:391,090-393,946	2.85	42.1	48.9	Serine/threonine-protein phosphatase 2A activator 2*(RRD2)*	CNBG_9459	10.6	Last exon (5th)
					Hypothetical protein	CNBG_4366	100	
					Hypothetical protein	CNBG_4365	23.4	Last exon (3th)
*cen10*Δ-D	Chr10:352,648-355,154	2.51	37.1	48	Ser/Thr protein kinase	CNBG_4379	88.4	
*cen10*Δ-E	Chr10:1-4,385	4.38	64.7	53.2	Hypothetical protein	CNBG_10450	100	
					Hypothetical protein	CNBG_4495	100	
*cen10*Δ-F	Chr10:342,517-345,159	2.64	39.0	45.5	Hypothetical protein	CNBG_4383	18.6	Last two exons
					Hypothetical protein	CNBG_10075	100	
					Hexokinase (HXK1)	CNBG_4382	15.3	Last three exons
*cen10*Δ-G	Chr10:378,389-386,366	7.97	117.7	46.5	High osmolarity signaling protein (SHO1)	CNBG_4373	100	
					Hypothetical protein	CNBG_4372	100	
					Hypothetical protein	CNBG_4371	100	
					Hypothetical protein	CNBG_4370	100	

Figures

Figure 1. Centromere deletion leads to neocentromere formation.

For each panel, the chromosome coordinates are indicated. Genes (CDS) are shown in blue arrows and the truncated transposable elements, located in the native centromere (*CEN9* or *CEN10*), are colored according to their class (*Tcn4* in orange and *Tcn6* in green). Previously generated RNA-sequencing obtained from wild-type cells was re-mapped and shown in green. In each panel, the wild-type CENP-A content is shown. In the wild type, CENP-A is only enriched at the native centromeres. For each *cen*Δ mutant, the neocentromeric region is shown by enrichment of CENP-A. (A) Schematic full overview of chromosome 9, the indentation represents the native centromere 9 position. The light grey area points to the zoomed-in chromosomal region shown with the detailed view of the native centromere (*CEN9*) and the location of the *cen9*Δ mutant neocentromeres. Neocentromeres of *cen9*Δ-B, *cen9*Δ-C and *cen9*Δ-E formed at the same chromosomal location. (B) Detailed view of the neocentromere of *cen10*Δ-B and the secondary CENP-A peak of *cen10*Δ-A and *cen10*Δ-C. (C) Overview of the chromosomal 10 region spanning 100 to 410 kb. *cen10*Δ-A and *cen10*Δ-C have two regions enriched with CENP-A (primary and secondary). (D) Schematic full overview of the full chromosome 10, the indentation represent the chromosomal location of the native centromere (*CEN10*). The light grey areas point to the zoomed-in chromosomal regions shown in panel C and below. The neocentromere of *cen10*Δ-E is indicated with an arrow. Lower panel, detailed view of the native centromere (*CEN10*) and the neocentromeres formed in *cen10*Δ-A, *cen10*Δ-C, *cen10*Δ-D, *cen10*Δ-F and *cen10*Δ-G mutants. (E) Detailed view of the telocentric neocentromere of *cen10*Δ-E.

Figure 2. Expression of neocentromeric genes.

Expression of the neocentromeric genes was assessed by qPCR for all *cen*Δ mutants and expression is shown as $Log2^{\Delta\Delta Ct}$. For *cen10*Δ-A, *cen10*Δ-B and *cen10*Δ-C, two genes were selected from each neocentromeric region, all other *cen*Δ mutants are represented by one gene spanned by CENP-A. *cen10*Δ-B has only one CENP-A-enriched region, and in this case,

the genes located within primary peak of *cen10*Δ-A and *cen10*Δ-C served as controls. The qPCRs of *cen10*Δ mutants are normalized with a housekeeping gene located on chromosome 10. The qPCRs of *cen9*Δ mutants are normalized with actin. Error bars show standard deviation.

Figure 3. *cen10*Δ mutant strains have reduced fitness compared to the wild-type strain. (A) Six out of seven *cen10*Δ mutants had a longer doubling time and slower growth than the wild-type strain. In contrast *cen10*Δ-E grows similarly to the wild type. Error bars show standard deviation. (B) Doubling times and fold change compared to wild type are shown. (C) Competition assays with the wild type and *cen9*Δ and *cen10*Δ mutant strains. Mixed cultures (1:1) were grown overnight and plated with and without selection agents. After four days, colonies were counted and the percentage of *cen*Δ mutants (black) and wild type (grey) in each culture was plotted. As a control (C) a wild-type strain with a *NAT* marker was mixed with the wild type.

Figure 4. *cen10*Δ mutants are aneuploid.

The whole genomes of small and large colonies derived from four *cen10*Δ mutants were sequenced and read coverage (corresponding to ploidy levels) was plotted. Small colonies of *cen10*Δ mutants were partially aneuploid for chromosome 10, while the large colonies are euploid. (A) Genome-wide read depth coverage for small and large colonies. On the right, the fold coverage for the highest ploidy level is indicated for each sample. For example, chromosome 10 of *cen10*Δ-B-S1 had an aneuploidy level of 1.35-fold compared to the wild-type strain. Chromosome 4 had a small region with increased read depth due to the ribosomal rDNA gene cluster and was excluded from the analysis. Chromosome 8 of *cen10*Δ-E was duplicated. In addition, *cen10*Δ-E-S3 had an additional duplicated region of 162 kb of chromosome 5 that spans the sequence of native centromere 5. (B) Detailed view of read depth of chromosome 10. As in panel A, read depth is indicated on the right. The native centromeric location is shown by a black square. Due to the deletion of

centromere 10, the location of the native centromere lacks sequence reads for each sample.

Figure 5. *cen10*Δ mutants undergo chromosome fusion leading to improved fitness at 37°C.

Chromosomal fusions were studied in detail for three *cen10*Δ mutants restored to wild-type growth levels at 37°C (large colonies). After chromosome fusion, the fused chromosomes of *cen10*Δ-A-L and *cen10*Δ-B-L lost the gene CNBG_6141, which is located in the 3' subtelomeric region of chromosome 10. Genes present in the fused chromosome are depicted in green, and genes lost after chromosome fusion are indicated in red. Gray highlights indicate regions present in both the parental and fused chromosomes. Each fusion occurred in a unique nonrepetitive region. (A) *cen10*Δ-A-L1, the fusion occurred between chromosome 10 and chromosome 4. (B) In *cen10*Δ-B-L1, chromosomal fusion occurred between chromosomes 10 and 7. (C) *cen10*Δ-E-L1 chromosomal fusion occurred between chromosomes 10 and 1.

Figure 6. Chromosome fusion results in neocentromere inactivation and karyotype reduction.

(A) Neocentromeres are inactive after chromosomal fusion. For each neocentromere two qPCR primer pairs located in genes spanned by the neocentromere in *cen10*Δ-A and *cen10*Δ-B mutant were used in a ChIP-qPCR experiment. Analyzed is the CENP-A enrichment of 1) a *cen10*Δ mutant, 2) a large colony derived from the *cen10*Δ mutant, and 3) the wild-type strain. Centromere 6 (*CEN6*) was included as a positive control, and actin was included as a negative control. Data is shown for *cen10*Δ-A, *cen10*Δ-A-L1, *cen10*Δ-B, *cen10*Δ-B-L2, and wild type. For *cen10*Δ-A and *cen10*Δ-A-L1 mutants, the chromosomal regions investigated are indicated according to the primary and secondary CENP-A peaks of the *cen10*Δ-A mutant. The *cen10*Δ-B mutant has only one CENP-A-enriched region which co-localized with the secondary CENP-A peak of *cen10*Δ-A and this region is labeled with neocen in *cen10*Δ-B and *cen10*Δ-B-L1 . Error bars show standard

deviation. (B) PFGE analysis shows that the band corresponding to chromosome 10 was lost in the large colonies and instead larger bands appear due to the fusion of chromosome 10 with other chromosomes. *cen10*Δ deletion mutants and small colonies derived from 37°C show a wild-type karyotype. Chromosome 10 of the large colonies was fused to chromosome 13, 10, or 1, respectively. Due to limitations of PFGE conditions, the chromosome 10–chromosome 1 fusion did not separate from chromosomes 2, 3, and 4. The positions of the fused chromosomes are indicated with arrows.

Figure 1

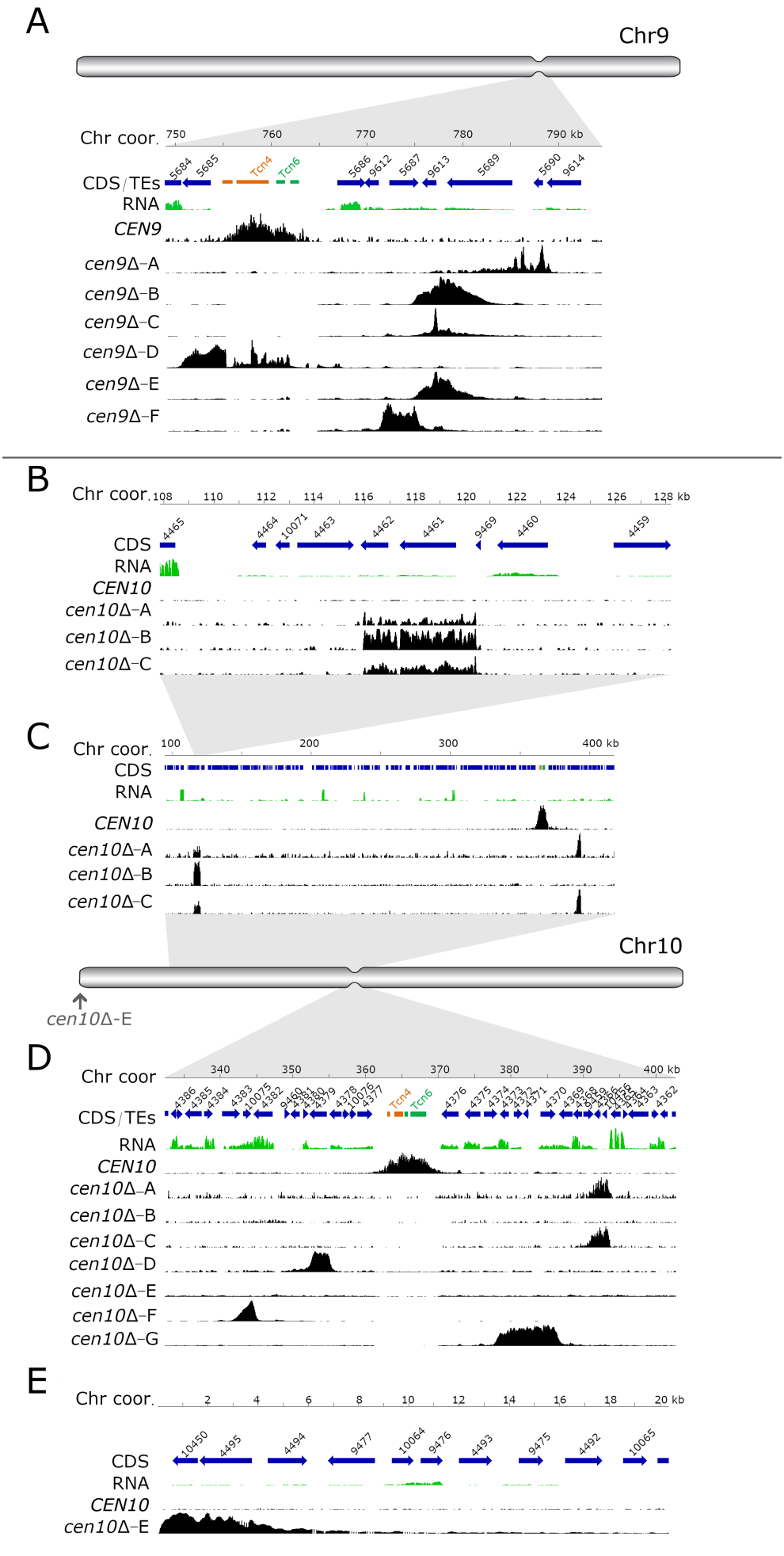

Figure 2

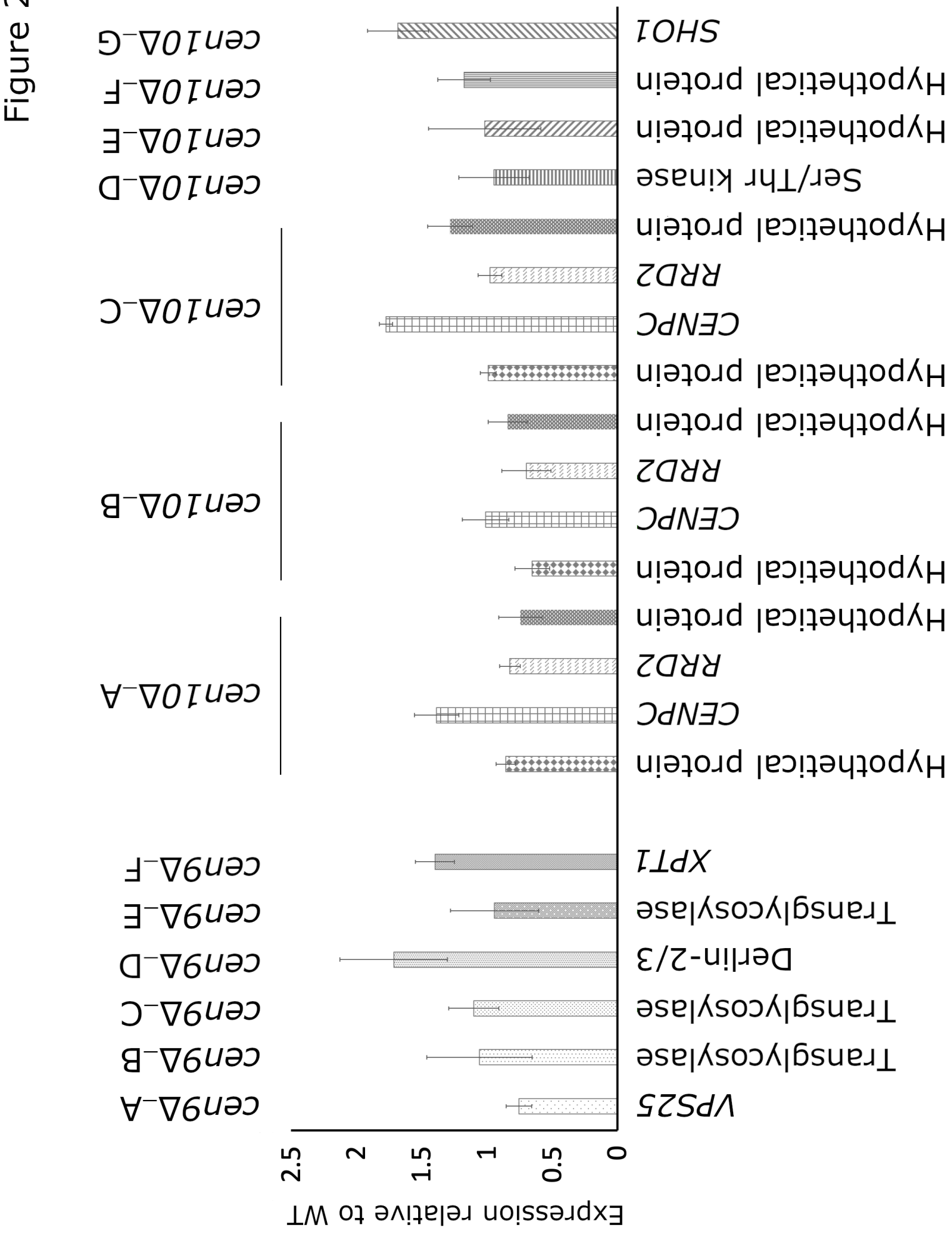

Figure 3

A

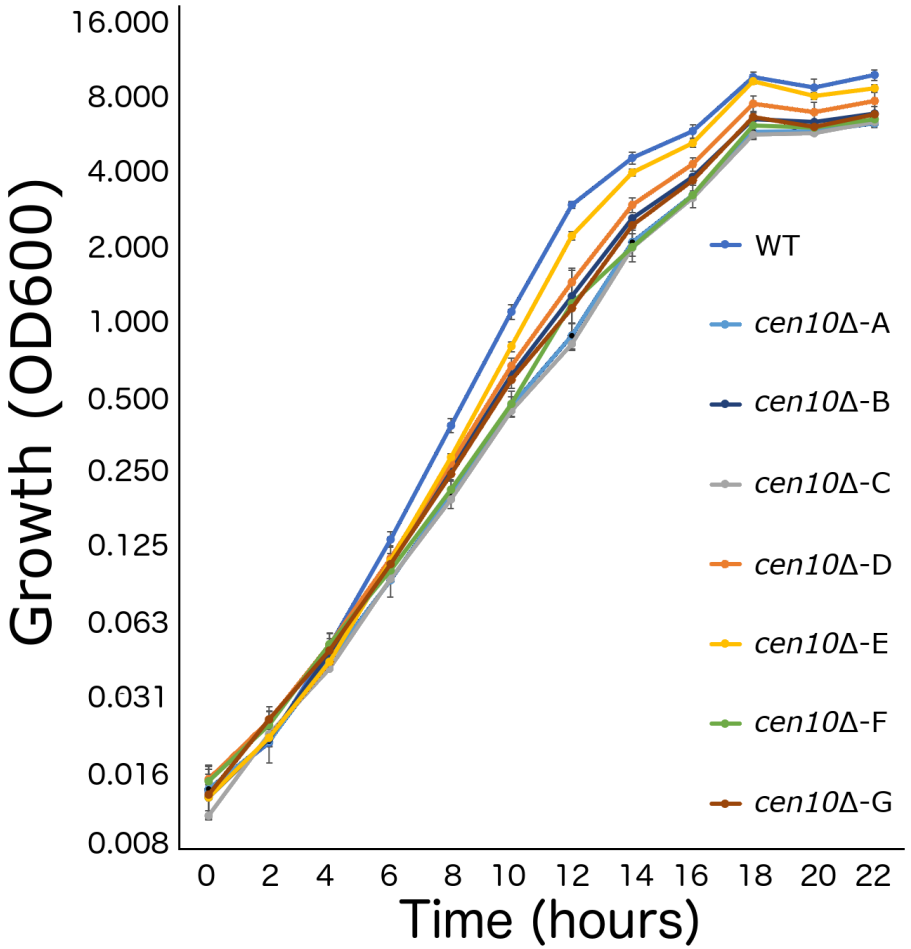

B

Isolate	Doubling time (min)	Relative to wild-type
WT	81	-
*cen10*Δ-A	111	1.4
*cen10*Δ-B	101	1.2
*cen10*Δ-C	111	1.4
*cen10*Δ-D	99	1.2
*cen10*Δ-E	84	1.0
*cen10*Δ-F	105	1.3
*cen10*Δ-G	105	1.3

C

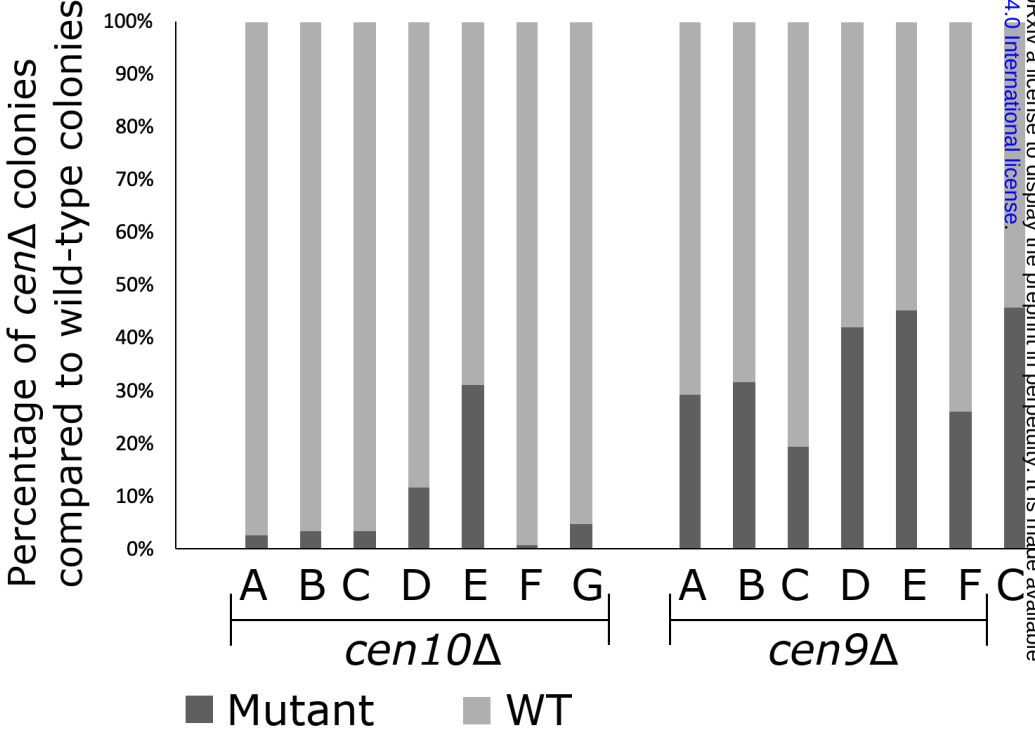

Figure 4

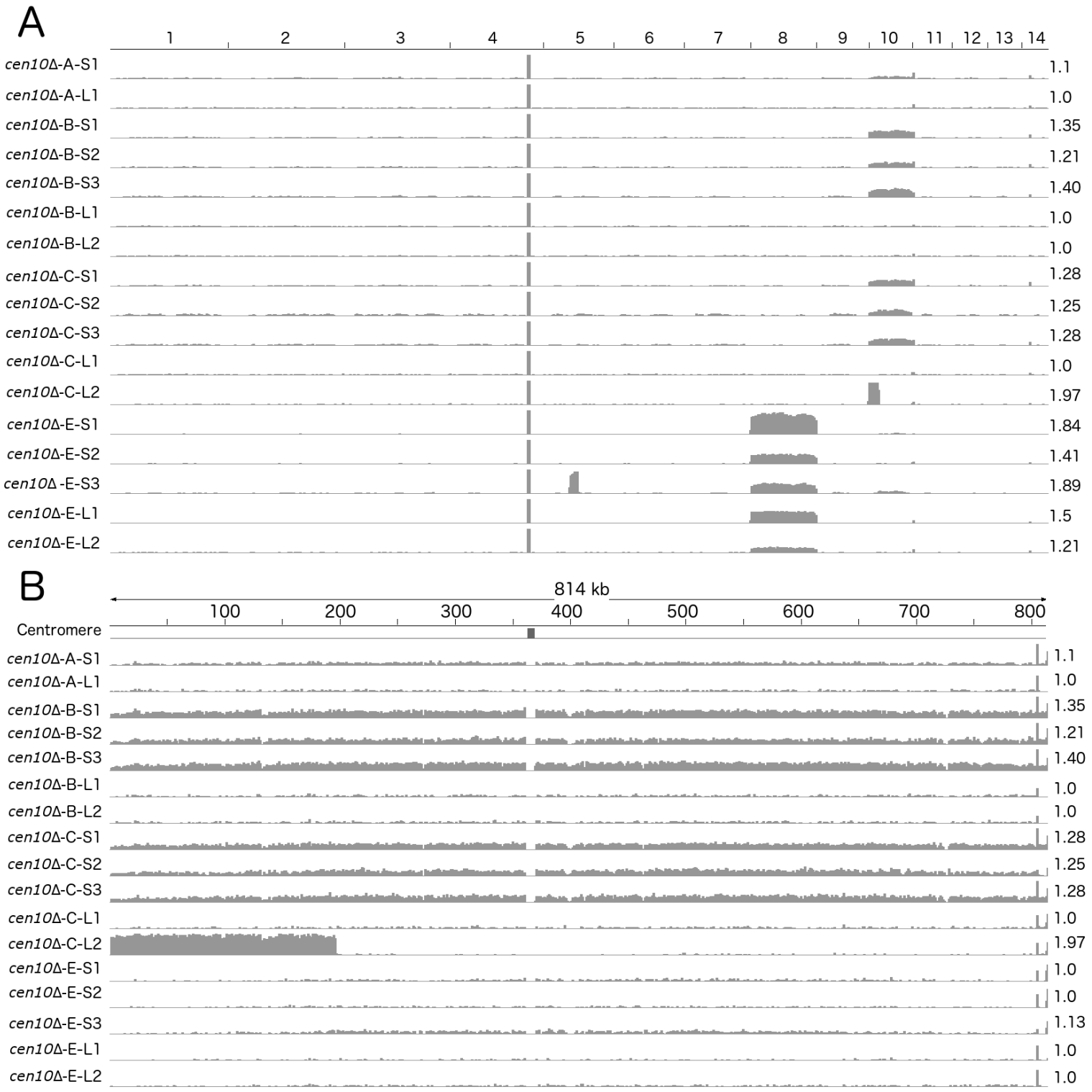

Figure 5

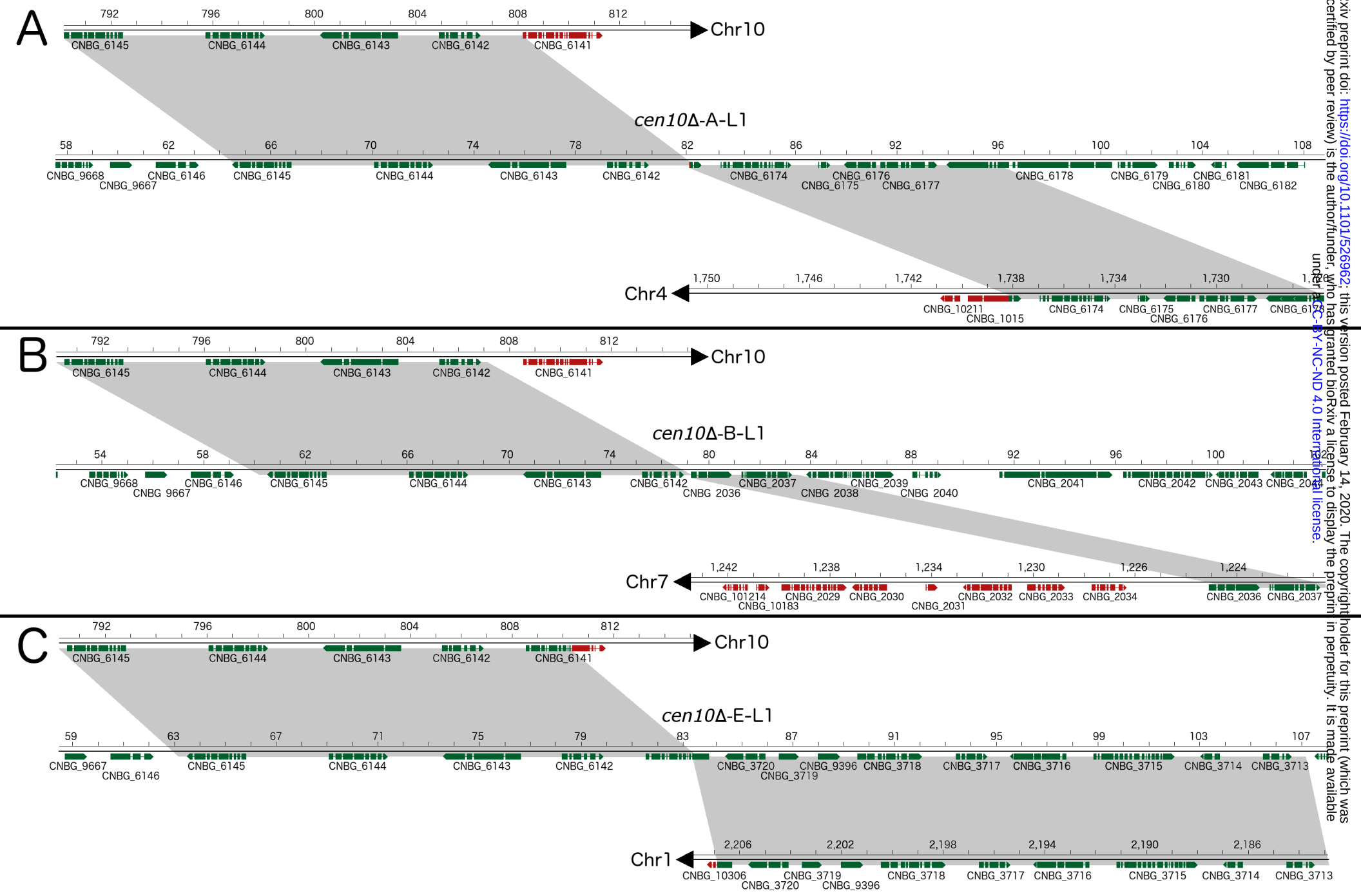

Figure 6

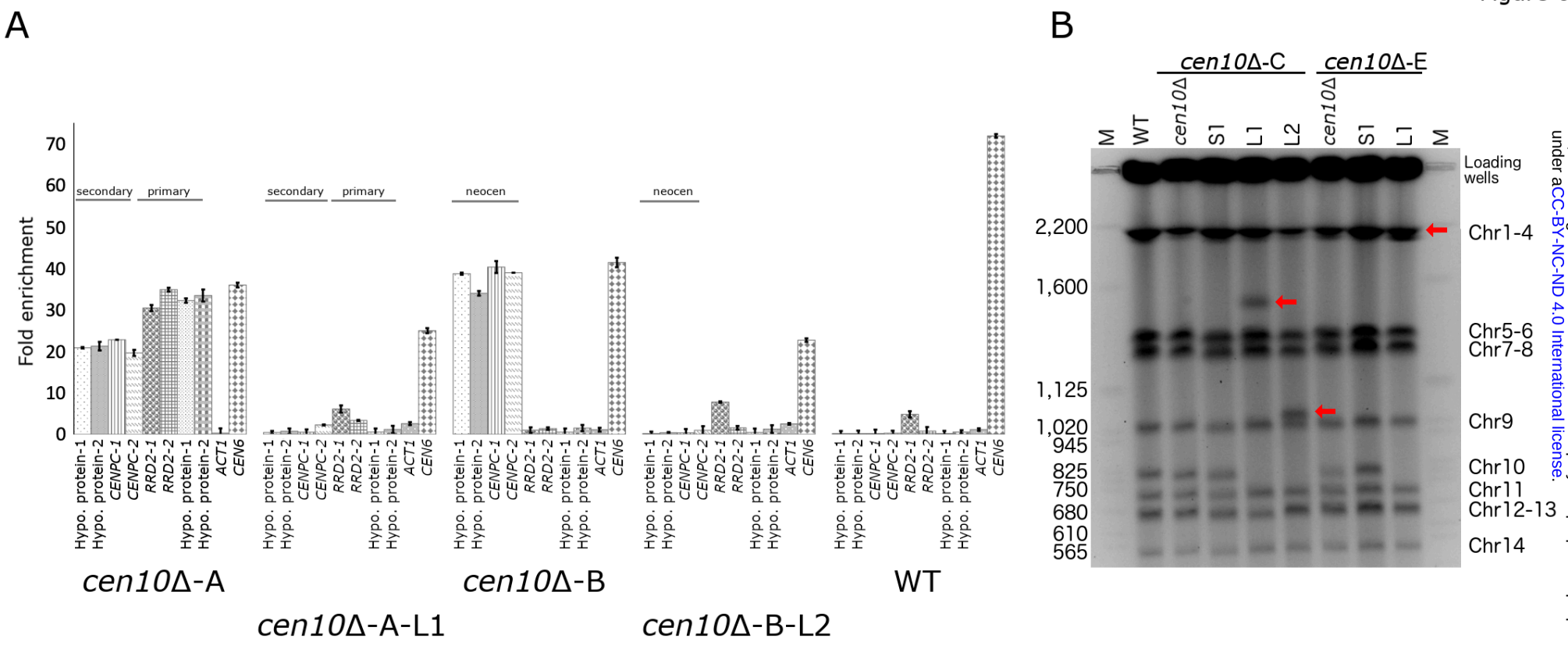

Supplementary figure legends

Supplementary figure 1. Confirmation of centromere 10 deletion by PCR (together with Figure 1).

(A) The native centromeric regions of chromosome 9 in the wild type and *cen9*Δ mutants are shown. Genes flanking the centromeric region in the WT strain are indicated with an arrow and gene ID. The centromere was replaced by a nourseothricin (*NAT*) drug-resistance gene cassette, indicated with a rectangle (labelled *NAT*). Black lines indicate the length of the PCR product used to confirm the centromere 9 deletion. Black arrows indicate primers. (B) PCR confirmation of the centromere 9 deletion in *cen9*Δ mutants ran on an ethidium bromide-stained gel. The WT (W) and no-template control (B) are included as controls. For the spanning PCR, both primers are located outside of the transformed product and for the junction PCRs, one primer is outside of the transformed product and one primer is located inside the nourseothricin (*NAT*) drug-resistance gene cassette. (C) Centromere 10 region of the wild type (WT) and *cen10*Δ mutants are shown. Genes and nourseothricin (*NAT*) drug-resistance gene cassette, primers, and the length of the PCR product are labeled as in A. (D) PCR confirmation of the centromere 10 deletion in *cen10*Δ mutants ran on an ethidium bromide-stained gel. The WT (W) and no-template control (B) are included as controls.

Supplementary figure 2. Centromere 10 is deleted in *cen10*Δ isolates (together with Figure 1).

(A) The region corresponding to the native centromere 10 of the wild type and *cen10*Δ mutants is shown. Upstream and downstream flanking regions, used for homologous recombination, are indicated with rectangles (labeled “5’ region” or “3’ region”). The nourseothricin drug resistance gene cassette is indicated with a rectangle, (labeled *NAT*). Grey lines indicate XbaI restriction sites. PCR products of the 5’ and 3’ regions were used as Southern blot probes, and the expected restriction pattern is indicated above. (B) Southern blot analysis for the wild-type and *cen10*Δ mutant strains is presented. Left panel shows the Southern blot, right panel shows the ethidium bromide-stained gel prior to

Southern blotting. Both the wild type and *cen10*Δ mutants have the expected restriction pattern which is shown in panel A.

Supplementary figure 3. *cen9*Δ and cen10Δ mutants have a wild-type karyotype (together with Figure 1, 5 and 6).

PFGE analysis with the wild type and *cen9*Δ and *cen10*Δ mutants. Cells were isolated from growing at 30°C. *S. cerevisiae* chromosomes serve as size markers and are indicated with "M" on both sides of the ethidium bromide stained gel (Chromosome sizes shown on the left side). The chromosome sizes of the reference strain R265 are shown on the right side. In several cases, chromosomes co-migrate as indicated.

(A) PFGE analysis of *cen10*Δ mutants. Order of samples from left to right are wild type and *cen10*Δ mutants (-A to -G). (B) Southern blot analysis of the PFGE from panel A. A region of *CEN10* served as the probe. On chromosome 10, the probe only has homology with the centromere. In the wild-type strain, the probe hybridized to chromosome 10 (arrow). *cen10*Δ mutants lack centromere 10 and thus do not show hybridization of the probe. The probe has homology to centromeres of other chromosomes, resulting in cross-hybridization. (C) PFGE analysis of *cen9*Δ mutants. Order of samples from left to right are *cen9*Δ mutants (-A to -D) and wild type.

Supplementary figure 4. ChIP-qPCR with additional kinetochore proteins

To confirm the binding of the kinetochore to the CENP-A-enriched regions, two additional kinetochore proteins were tagged with GFP and ChIP-qPCR analysis was performed. *cen9*Δ mutants were transformed with a construct expressing CENP-C-GFP and *cen10*Δ mutants were transformed with a construct expressing Mis12-GFP. As a control, the wild type was transformed with a construct expressing CENP-C-GFP or Mis12-GFP. For each, ChIP-qPCR data is shown for 1) the internal positive control (*CEN6*), 2) primer pair(s) specific for the neocentromere(s) and 3) enrichment compared to actin (set to 1). Error bars show standard deviation. (A) qPCR results of the ChIPs with c*en10*Δ mutants transformed with Mis12-GFP. *cen10*Δ-A and *cen10*Δ-C have two CENP-A-enriched regions (primary peak and

secondary peak) and this is indicated in the figure. B) qPCR results of ChIPs with *cen9*Δ mutants transformed with CENP-C-GFP. C) qPCR results of the ChIP with the wild-type strain transformed with Mis12-GFP. This panel serves as a control for the ChIP-qPCRs performed in panel A. As the neocentromere of *cen10*Δ-B and the secondary peak of *cen10*Δ-A and *cen10*Δ-C are formed in the same chromosomal region, the qPCR reaction for this chromosomal region in the wild type is only shown once. Similarly, the primary peak of *cen10*Δ-A and *cen10*Δ-C formed in the same chromosomal location, and this region is only shown once in the wild type. D) qPCR results of the ChIP with the wild-type strain transformed with CENP-C-GFP. These qPCRs serve as a control for the ChIP-qPCRs performed in panel B. Three mutants have neocentromeres formed at the same chromosomal location (*cen9*Δ-B, *cen9*Δ-C and *cen9*Δ-E) and the CENP-C enrichment of this region in the wild type is only shown once.

Supplementary figure 5. *cen10*Δ mutants with chromosomal fusion have a wild-type growth rate (together with Figure 3 and 6).

The doubling times of large and small colonies derived from *cen10*Δ mutants at 30^{o}C were determined. Large colonies had a growth rate similar to the wild-type strain, while small colonies and the initial *cen10*Δ mutants had a similar growth rate with one another but that was slower than the wild-type strain and the derived large colonies. (A) Growth curves for *cen10*Δ-A-derived isolates and the wild-type strain are shown. (B) Growth curves for *cen10*Δ-B-derived isolates and the wild-type strain are shown.

Supplementary figure 6. Deletion within subtelomeric regions in chromosome fusion isolates (together with Figure 4 and 6).

Sequence reads were mapped to the reference R265 genome. Regions with sequence coverage are shown in blue, and those without sequence coverage are shown in white. Subtelomeric regions of the large *cen10*Δ colonies have lost sequence coverage, whereas *cen10*Δ small colonies have wild-type sequence coverage. Telomeric loss was not observed for the large colonies of *cen10*Δ-E. For all panels, genes (CDS) are shown on the top (light

blue). (A) Detailed view of the 3' subtelomeric region of chromosome 10. Large colonies of *cen10*Δ-A and *cen10*Δ-B lost sequences corresponding to a region of 6.5 and ~8 kb. (B) Detailed view of the 3' subtelomeric region of chromosome 4. Large colonies of *cen10*Δ-A have lost sequences corresponding to a 12-kb region. (C) Detailed view of the 3' subtelomeric region of chromosome 7. Large colonies of *cen10*Δ-B lost sequences corresponding to an ~18.5-kb region.

Supplementary figure 7. Chromosome fusion in large *cen10*Δ colonies (together with Figure 5).

Sequence reads were mapped back to the *de novo cen10*Δ genome assemblies to verify the quality of the *de novo cen10*Δ mutant genome assemblies. For each panel the full length of the scaffold, which includes the fusion point, and a 100-bp detailed region is shown. Sequences homologous to chromosome 10 are depicted in blue and sequence reads mapped back to the *de novo* genome assemblies are shown in grey. (A) The *de novo* genome assembly of *cen10*Δ-A-L contains a scaffold (~211 kb) of a fused chromosome and this scaffold consists of an 81.97-kb region of chromosome 10 (blue) and a 129.38-kb region of chromosome 4 (green). The sequence coverage of this scaffold is 104 fold. The chromosome fusion occurred with a 2-bp overlap between chromosome 4 and 10. (B) The *de novo* genome assembly of *cen10*Δ-B-L contains a scaffold (~886 kb) and consists of an 80.46-kb region of chromosome 10 (blue) and an 806.09-kb region of chromosome 7 (red). The fusion point lacks overlap between chromosomes 7 and 10. The sequence coverage of this scaffold is 104 fold. (C) The *de novo* genome assembly of *cen10*Δ-E-L consists of a scaffold (~585 kb) of a fused chromosome and this scaffold consists of an 83.59-kb region of chromosome 10 (blue) and 501.37-kb of chromosome 1 (pink). The sequence coverage of this scaffold is 140 fold. The chromosome fusion occurred with a 6-bp overlap between chromosome 1 and 10. (D) PCR confirmation of the chromosome fusion occurring in the large colonies derived from *cen10*Δ-B, *cen10*Δ-C, and *cen10*Δ-A. For each chromosomal fusion, a PCR spanning the fusion was performed. For each chromosome fusion, PCRs were

performed for: 1) a large colony derived from the *cen10*Δ mutant, 2) the original *cen10*Δ mutant, 3) a small colony derived from growth at 37°C, and 4) the wild type.

Supplementary figure 8. *cen10*Δ mutants have elongated cell morphology (together with Figure 1).

Cell morphology of >1000 cells each for the wild-type strain and five *cen10*Δ mutant strains was analyzed, counted, and plotted as a percentage of total cell number. L = large, S = small, Scale bar = 10 μm. (A) Percentage of cells with elongated cell morphology. Formation of abnormal cell morphology is rare. The *cen10*Δ-C and *cen10*Δ-F mutants have an increased number of elongated cells. *cen10*Δ-D, *cen10*Δ-E, and *cen10*Δ-G mutants had <0.5% elongated cell morphology. (B) Representative view of wild-type and *cen10*Δ-F mutant cells. Several *cen10*Δ-F mutants had enlarged cell shapes and formed elongated cell clusters. (C) Representative view of wild-type colonies and a population of mixed colony sizes of *cen10*Δ mutants. Shown here is *cen10*Δ-A. Large colonies have a size to similar to wild type.

Figure S1

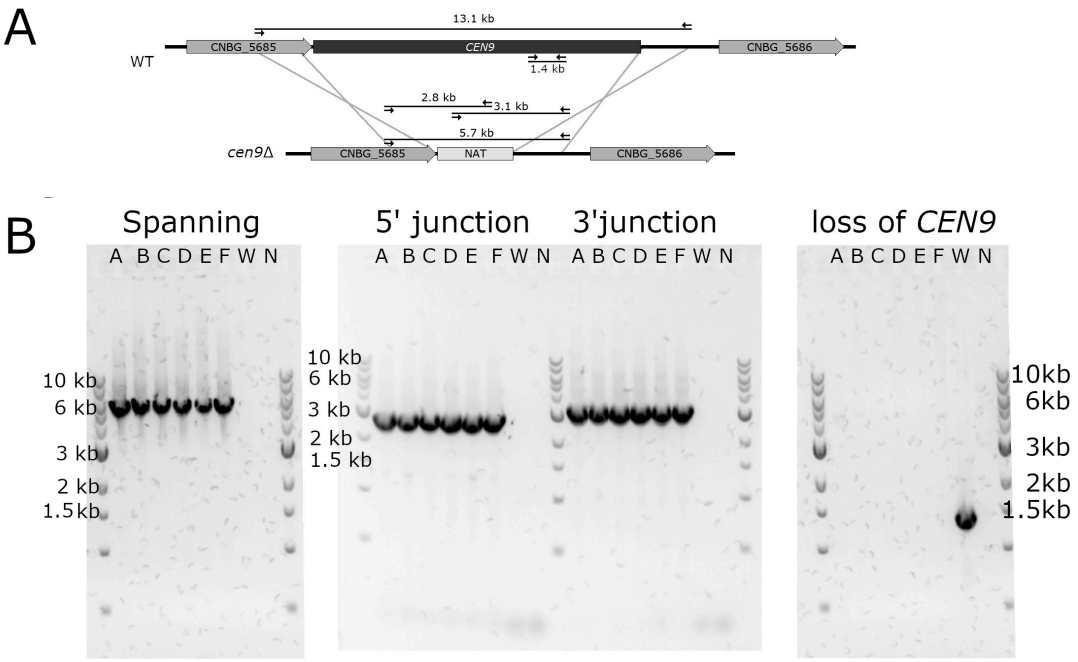

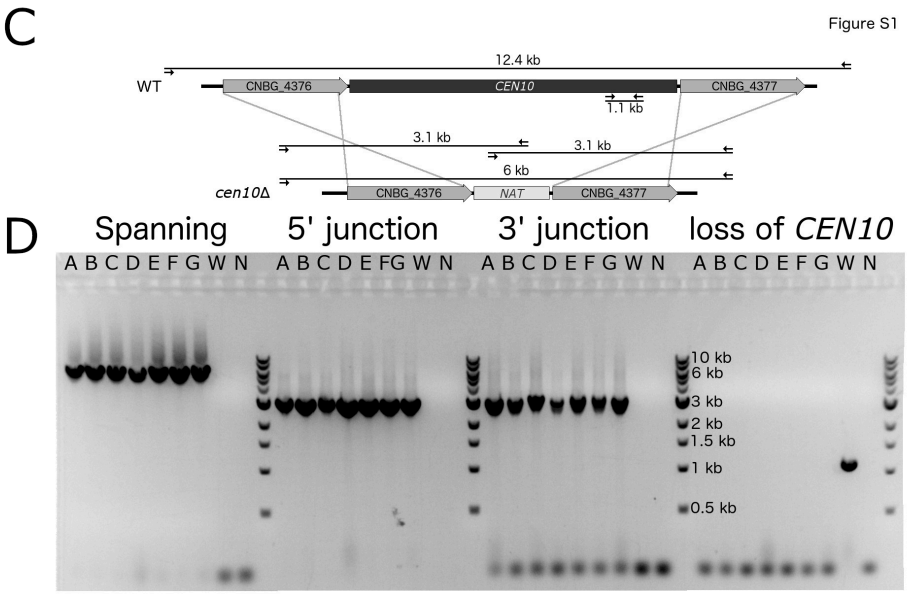

Figure S2

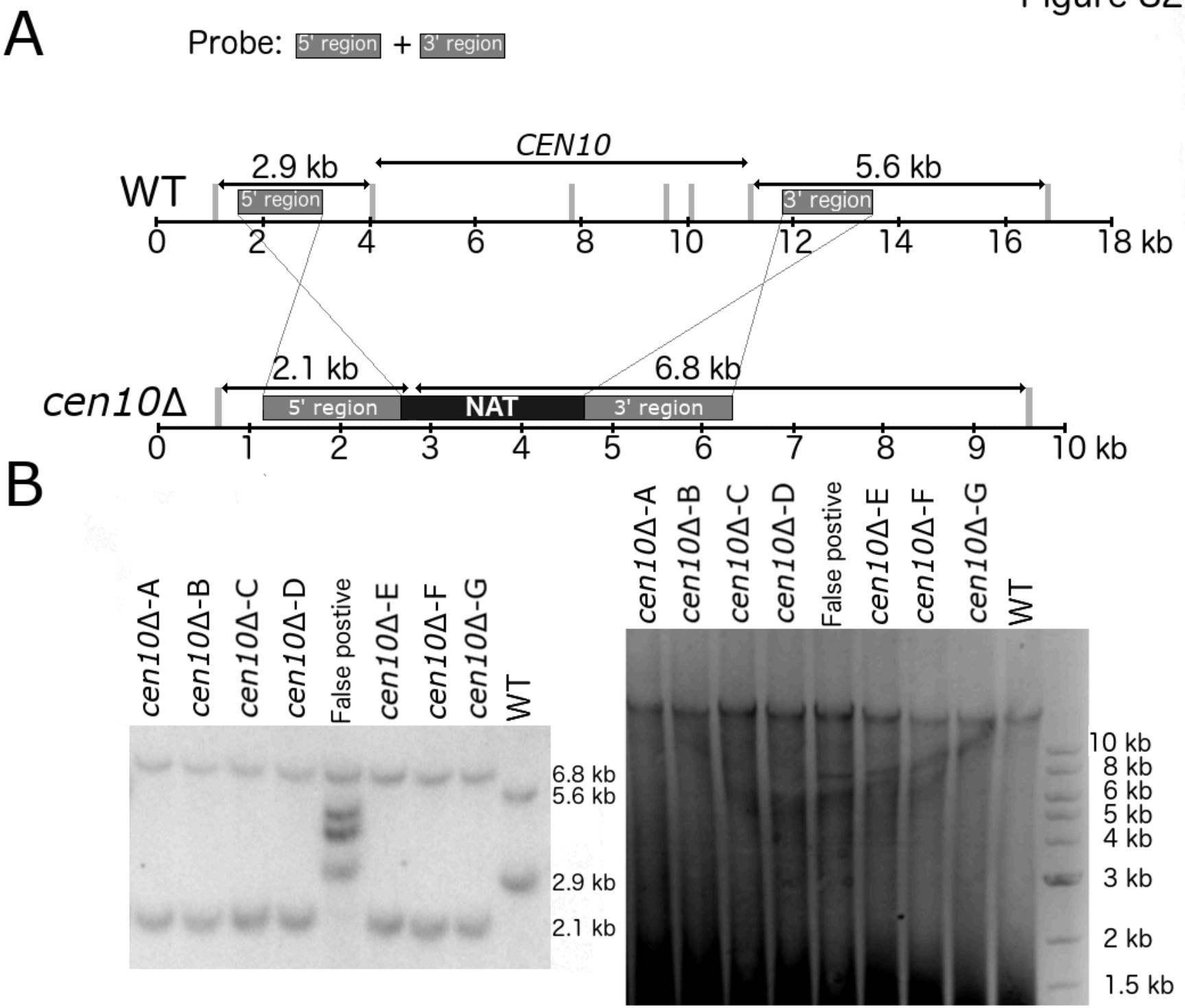

Figure S3

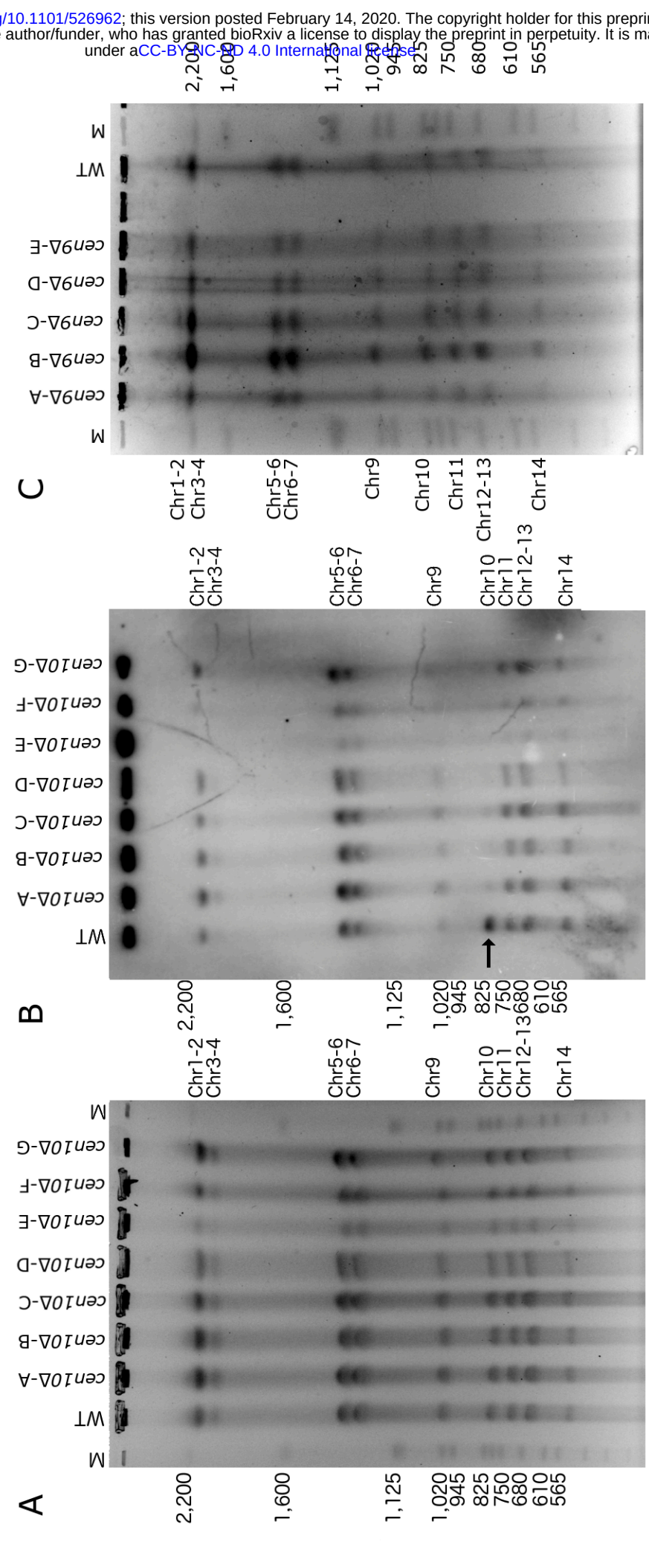

Figure S4

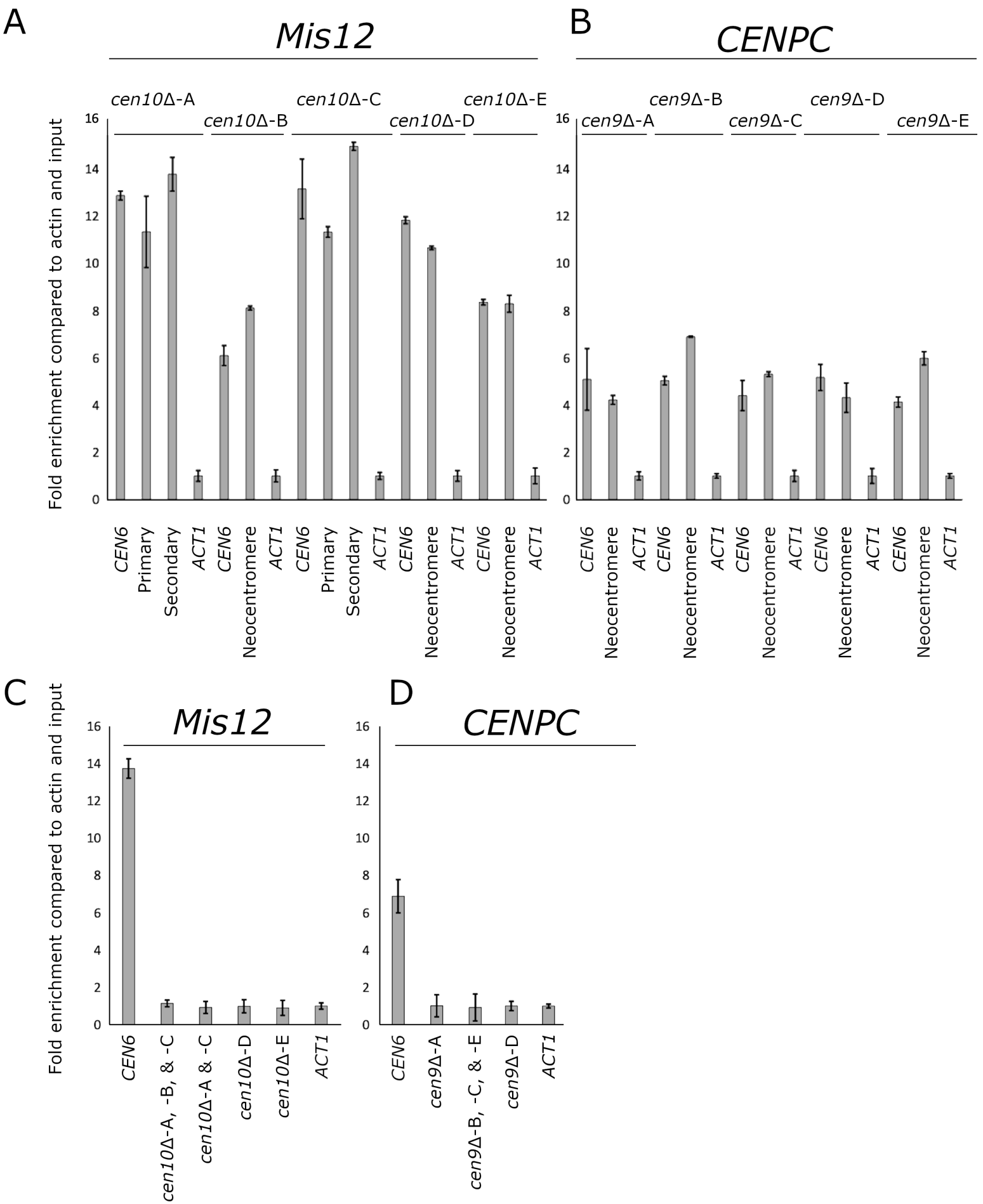

Figure S1

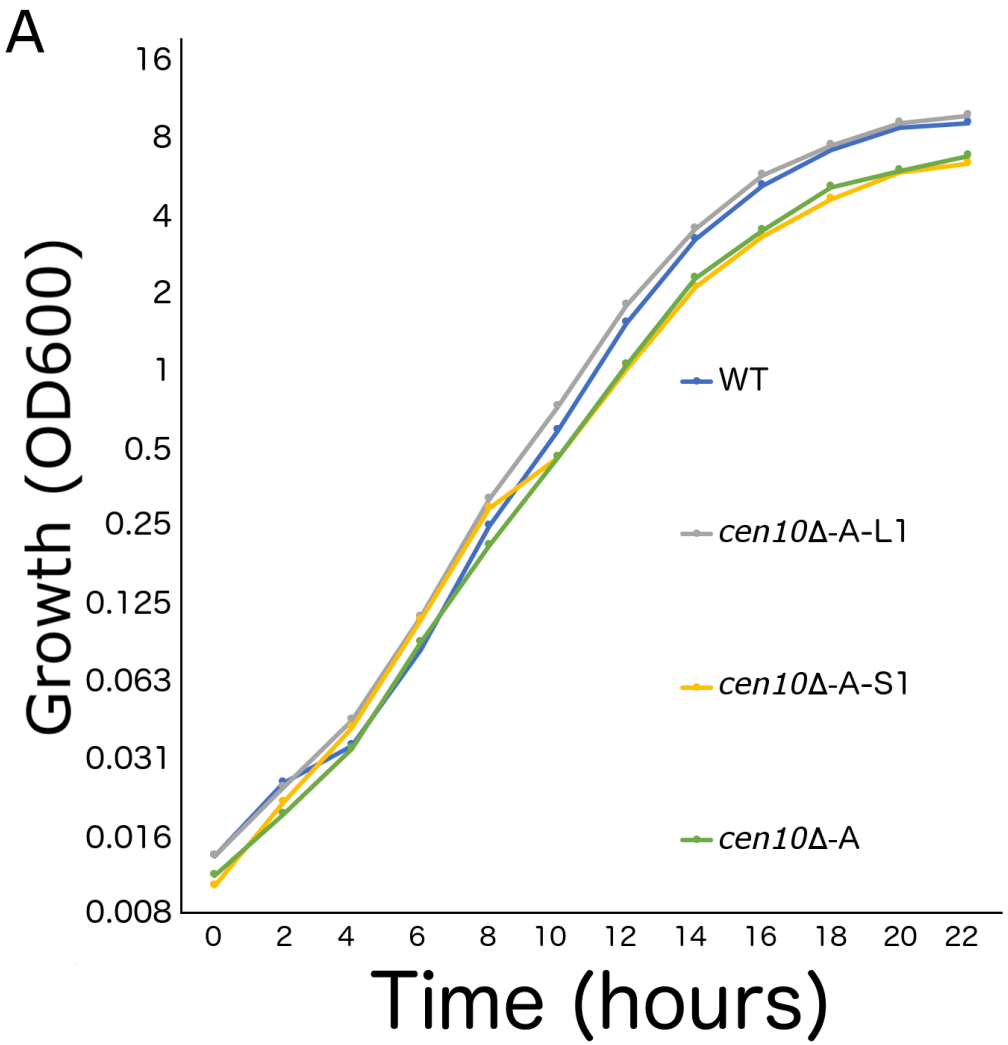

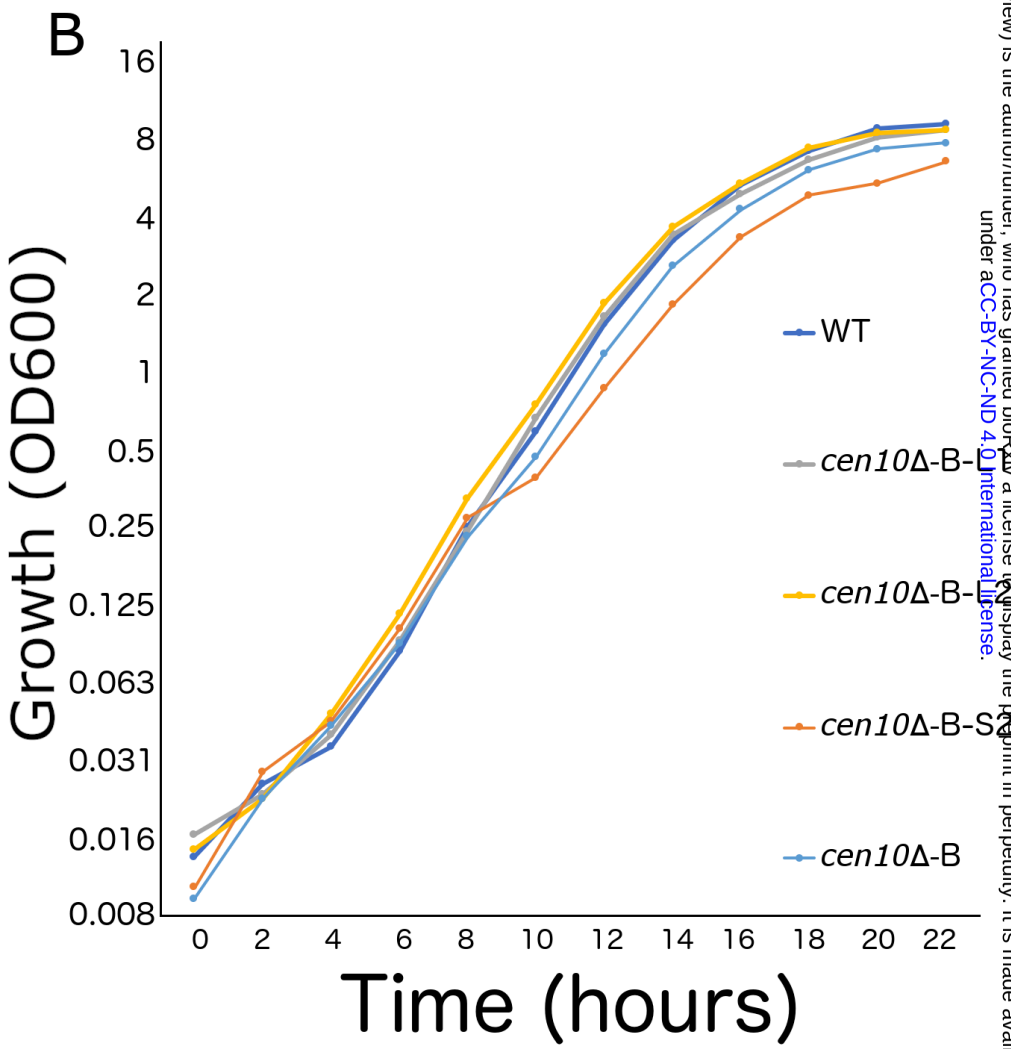

Figure S6

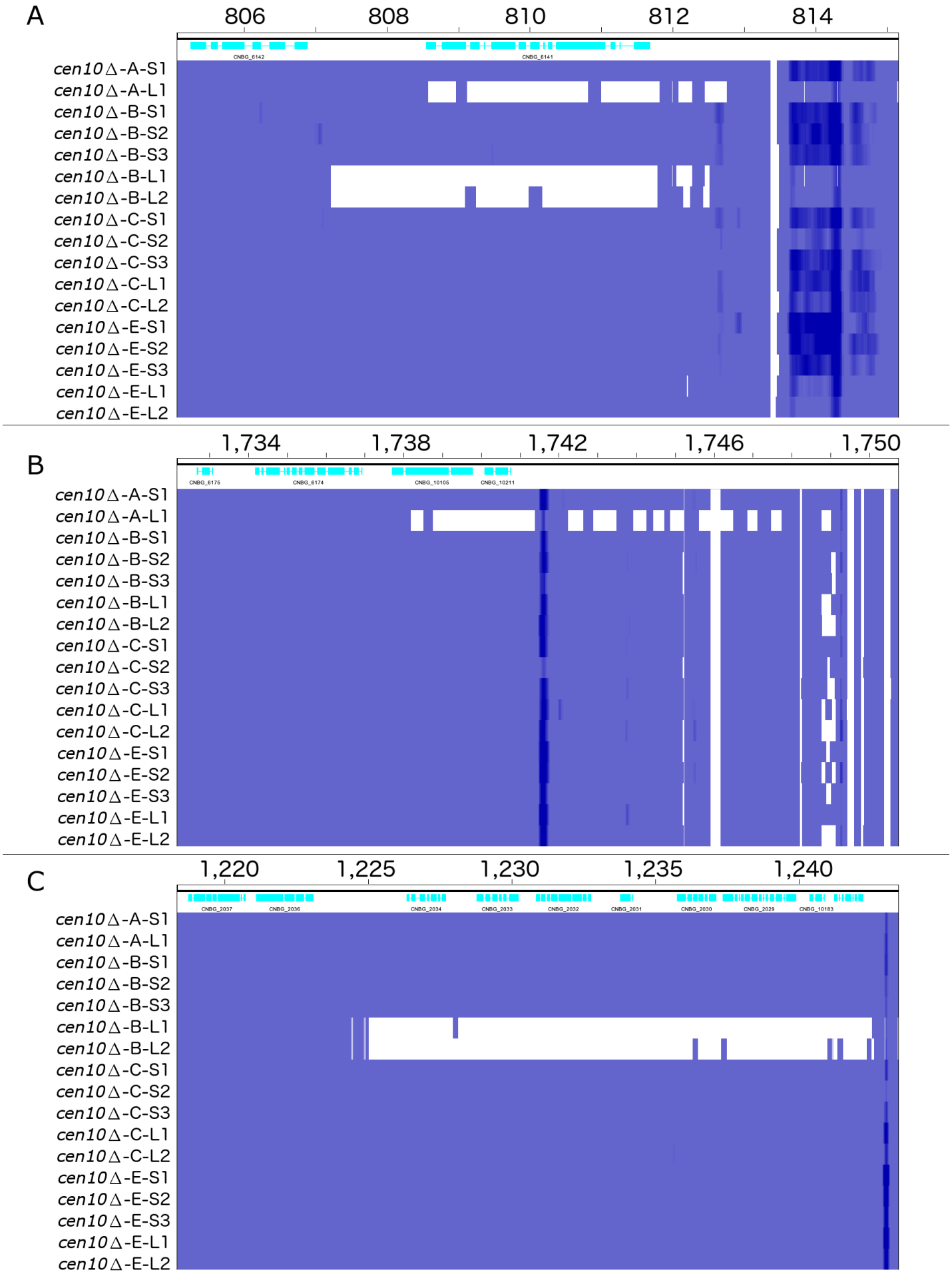

Figure S7

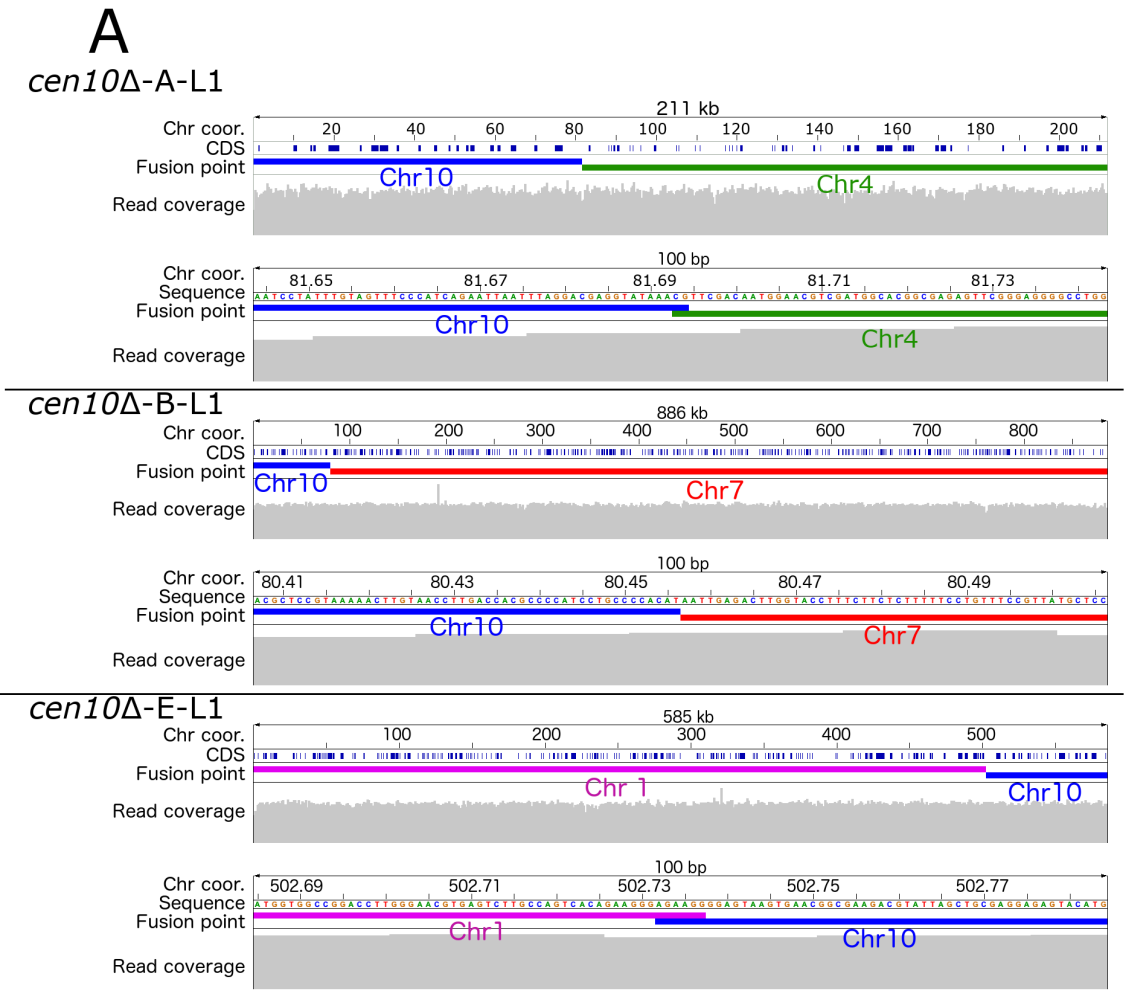

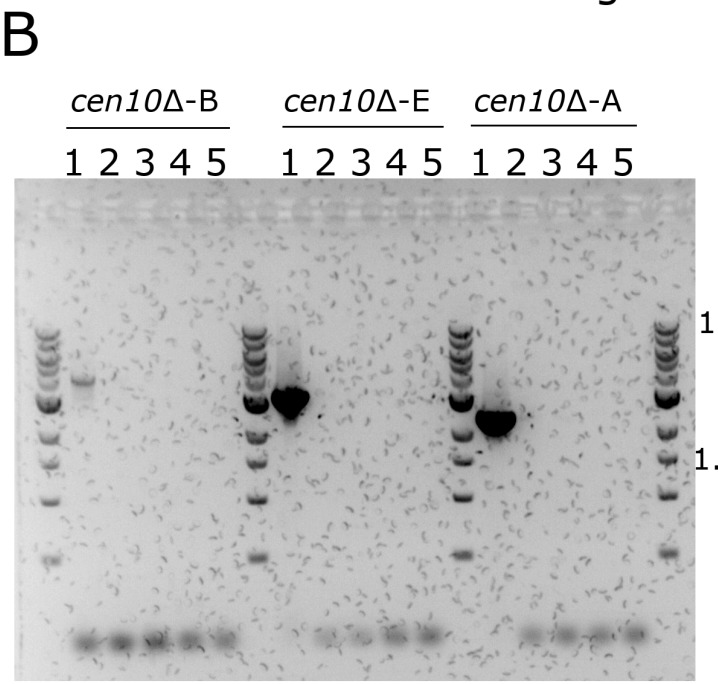

1) Large *cen10*Δ colony (Chromosome fusion)
2) Original *cen10*Δ mutant
3) Small *cen10*Δ colony
4) Wild-type
5) No-DNA control

Expected size of PCR for chromosome fusion:

*cen10*Δ-B	4.1 kb
*cen10*Δ-E	3.1 kb
*cen10*Δ-A	2.4 kb

Figure S8

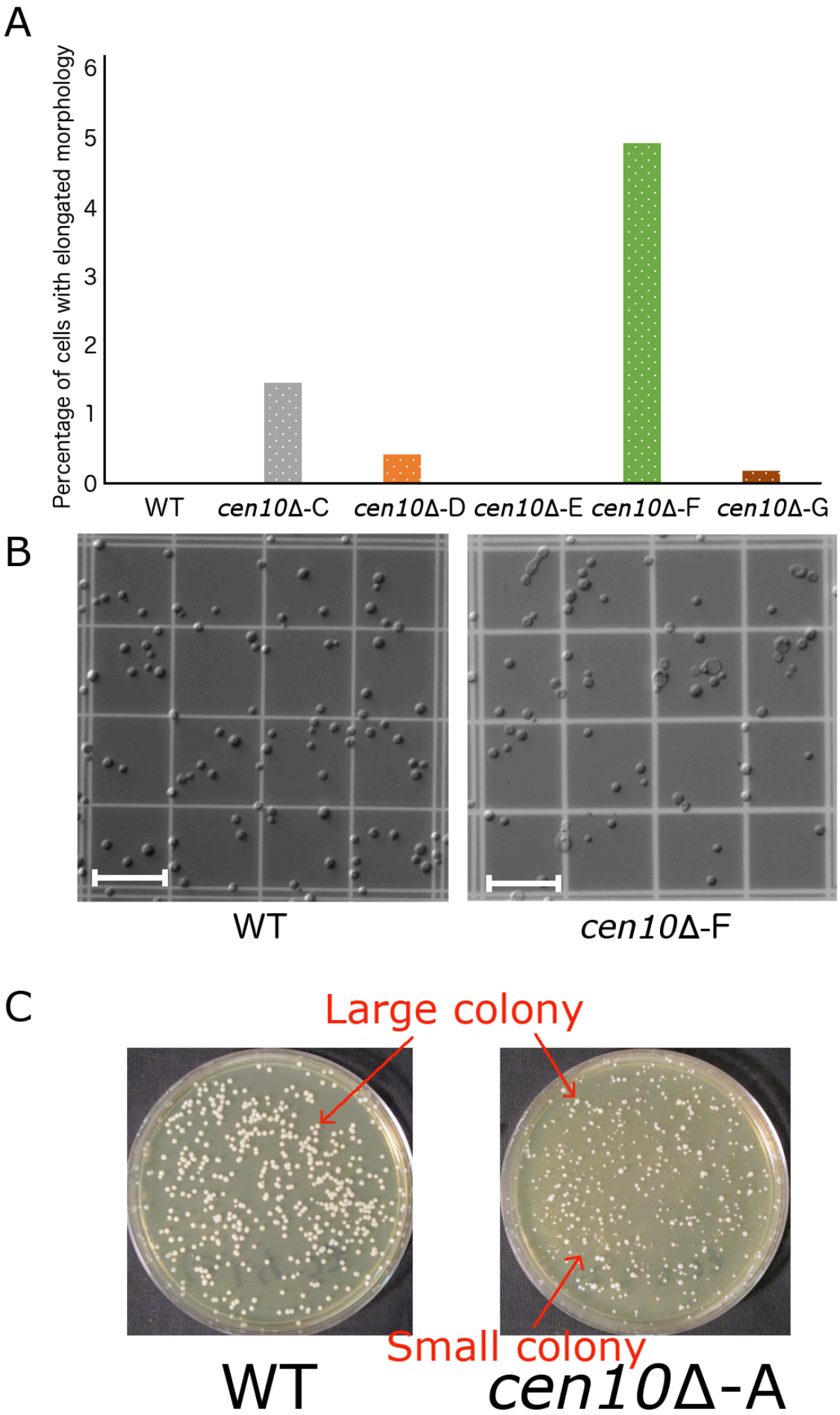

Supplementary Table 1. Primers used in this study.

# Primer Heitman lab	Primer	Sequence	Purpose of primers
JOHE44300/KS29	M13_FWD	CGCCAGGGTTTTCCCAGTCACGAC	primers to delete *CEN10*
JOHE44301/KS30	M13_REV	AGCGGATAACAATTTCACACAGGA	primers to delete *CEN10*
JOHE44961/KS398	*Cen10* △_UF_FWD	GAACGCACTGGCAATGTGGA	primers to delete *CEN10*
JOHE44962/KS399	*Cen10* △_UF_REV	GTCGTGACTGGGAAAACCCTGGCGGATGGATTCCCCCAGCTCTT	primers to delete *CEN10*
JOHE44963/KS400	*Cen10* △_DF_FWD	TCCTGTGTGAAATTGTTATCCGCTGCATCATGCCATTCAGCCCT	primers to delete *CEN10*
JOHE44964/KS401	*Cen10* △_DF_REV	GGTGCAATCGGTTTGGAAGG	primers to delete *CEN10*
JOHE44965/KS402	*Cen10* △_Nested_FWD	GAACGCACTGGCAATGTGGA	primers to delete *CEN10*
JOHE44966/KS403	*Cen10* △_Nested_REV	GGTGCAATCGGTTTGGAAGG	primers to delete *CEN10*
JOHE44967/KS404	*Cen10* △_Inner_FWD	CCAAAAACTGCCCCATGCAC	primers to delete *CEN10*
JOHE44968/KS405	*Cen10* △_Inner_REV	TGTATGCTGCCGGTTTCCCT	primers to delete *CEN10*
JOHE44969/KS406	*Cen10* △_Out_FWD	TGCTTTGCGGACCAAGTGAG	primers to delete *CEN10*
JOHE44970/KS407	*Cen10* △_Out_REV	GCAAGCACCTTGGATGGCAA	primers to delete *CEN10*
JOHE45241/KS422	CEN10_probe_Fwd	GCAGCGGAATAATGGGTGGA	primers to delete *CEN10*
JOHE45242/KS423	CEN10_probe_Rev	CGATTCAATCTGGCAAGGGG	primers to delete *CEN10*
JOHE45316/KS433	T44_UF_Rev	TCCTCGCCCTTGCTCACCATTCTCCTACTCTTCCCTTTACTTTTTCTCTTC	CENPC construct
JOHE45317/KS434	T44_DF_Fwd	GTCGTGACTGGGAAAACCCTGGCGCGATAACCTGATCTGCGCGT	CENPC construct
JOHE45318/KS435	T44_DF_Rev	GAGCGAATGATGCGAAGACG	CENPC construct
JOHE45319/KS436	T44_nested_UF	CAGCGTTGTTCATCCTGCCA	CENPC construct
JOHE45320/KS437	T44_nested_DF	CGTCCAAACCTCCAAAACCG	CENPC construct
JOHE45381/KS454	1_Fwd	GCAGATGCATACAAAGCCCC	*CEN10* test primers
JOHE45382/KS455	1_Rev	GCAGTGGAACAACGGTGGA	*CEN10* test primers
JOHE45383/KS456	2_Fwd	GGTTGGCCTGGAAGTCTTTG	*CEN10* test primers
JOHE45384/KS457	2_Rev	CCGTCTTTGTATGGGGCAGA	*CEN10* test primers
JOHE45385/KS458	3_Fwd	CATCTGGATTCCACTGGGCT	*CEN10* test primers
JOHE45386/KS459	3_Rev	ATGCTGCCGGTTTCCCTGTT	*CEN10* test primers
JOHE45387/KS460	4_Fwd	CGATTCAATCTGGCAAGGGG	*CEN10* test primers
JOHE45388/KS461	4_Rev	TTGGTGGTAAGGGCTCTGCA	*CEN10* test primers
JOHE45389/KS462	5_Fwd	TGATGCAGATTGGGGAGGAG	*CEN10* test primers
JOHE45390/KS463	5_Rev	TCCACCCATTATTCCGCTGC	*CEN10* test primers
JOHE45391/KS464	6_Fwd	GGATCAAGGGGGAGTGTTGGA	*CEN10* test primers
JOHE45392/KS465	6_Rev	CGGTGTGGCAAGCTTTTTGC	*CEN10* test primers
JOHE45393/KS466	7_Fwd	TGCTTCGTTGATACGGCGCT	*CEN10* test primers
JOHE45394/KS467	7_Rev	ACTGGGTGCCTCACTGAGTGT	*CEN10* test primers
JOHE45395/KS468	8_Fwd	CAGCCAGATGATGTGGCATTC	*CEN10* test primers
JOHE45396/KS469	8_Rev	TGTGCATTGTCACTGGCCCA	*CEN10* test primers
JOHE45397/KS470	9_Fwd	ATCTTGGGGTGGAGGGAGGAT	*CEN10* test primers
JOHE45398/KS471	9_Rev	GCAGATGCTGGCACAAAGCA	*CEN10* test primers
JOHE45409/KS474	T44_Mcherry_Fwd	GAAGAGAAAAAGTAAAGGGAAGAGTAGGAGAAGAATGGTGAGCAAGGGCGAG	CENPC construct
JOHE45410/KS475	T44_Mcherry_Rev	TCCTGTGTGAAATTGTTATCCGCTACCCAGCATCCAGCATCCAA	CENPC construct
JOHE45411/KS476	T44_UF_Rev_mcherry	CTCGCCCTTGCTCACCATTCTTCTCCTACTCTTCCCTTTACTTTTTCTCTTC	CENPC construct
JOHE45636/KSS01	CEN6_Fwd1	GCCAACAAGGGTTTCCACCA	*CEN6* control primers
JOHE45637/KSS02	CEN6_Rev1	AAGCGCTGGAAAACAGCAGG	*CEN6* control primers
JOHE45780/KSS07	mCherry-CENPA_gene_Fwd	GCATGGACGAGCTGTACAAGGGTGGCGGTGGCATGGCAAGAACAGTAACGAGCCC	mCherry-CENPA
JOHE45781/KSS08	mCherry-CENPA_gene_Rev	GTGTGAAATTGTTATCCGCTCACGGACATGGAACACGGAT	mCherry-CENPA
JOHE45782/KSS09	mCherry-CENPA_UF-Prom_Fwd	TTTGAGGACTGGCTTGCGGA	mCherry-CENPA
JOHE45783/KSS10	mCherry-CENPA_UF-Prom_Rev	TCCTCGCCCTTGCTCACCATCCCTCTGATCGCTTCGTTGA	mCherry-CENPA
JOHE45784/KSS11	mCherry-CENPA_DF_Fwd	TGACTGGGAAAACCCTGGCGATCCGTGTTCCATGTCCGTG	mCherry-CENPA
JOHE45785/KSS12	mCherry-CENPA_DF_Rev	TCATCCCCTTCTTGCTCGCA	mCherry-CENPA
JOHE45786/KSS13	mCherry_Fwd	TCAACGAAGCGATCAGAGGGATGGTGAGCAAGGGCGAGGA	mCherry-CENPA
JOHE45787/KSS14	mCherry_Rev	GGGCTCGTTACTGTTCTTGCCATGCCACCGCCACCCTTGTACAGCTCGTCCATGC	mCherry-CENPA
JOHE45788/KSS15	mCherry-CENPA_nested_Fwd	ACAAATCCGGGGGCAACTTC	mCherry-CENPA
JOHE45789/KSS16	mCherry-CENPA_nested_Rev	TTGAGGCTGGCGAGAAGGAA	mCherry-CENPA
JOHE46266/KS565	CNBG_4355_1_Fwd	TCCAGGTTTCTGGGCTAAAG	Genes in neocentromere
JOHE46267/KS566	CNBG_4355_1_Rev	CGGACTCCCACACTTGATCT	Genes in neocentromere
JOHE46268/KS567	CNBG_4355_2_Fwd	AGTCGGACGATTCACCTTTG	Genes in neocentromere
JOHE46269/KS568	CNBG_4355_2_Rev	CCCCACCATGCTTACTTGAT	Genes in neocentromere
JOHE46270/KS569	CNBG_9459_1_Fwd	CCATTCACGACCCAGAAGTT	Genes in neocentromere
JOHE46271/KS570	CNBG_9459_1_Rev	CCACGTTTTGACAGCAGAGA	Genes in neocentromere
JOHE46272/KS571	CNBG_9459_2_Fwd	TCTTGGGAAAATTGCCTGTC	Genes in neocentromere
JOHE46273/KS572	CNBG_9459_2_Rev	TCAAGAGCCCTTTCAGCTC	Genes in neocentromere
JOHE46274/KS573	CNBG_4462_1_Fwd	TCGATAAATGGGCGAAGAC	Genes in neocentromere
JOHE46275/KS574	CNBG_4462_1_Rev	CGCCAGGTAGATGAGGAGAG	Genes in neocentromere
JOHE46276/KS575	CNBG_4462_2_Fwd	CCCTACCTACGACGCTCTTG	Genes in neocentromere
JOHE46277/KS576	CNBG_4462_2_Rev	TGCCTGTTTCACTTCACTCG	Genes in neocentromere
JOHE46278/KS577	CNBG_4461_1_Fwd	AATTCCTCGTCCCAAGAGGT	Genes in neocentromere
JOHE46279/KS578	CNBG_4461_1_Rev	CTCTCCCGCTTGAGATTCTG	Genes in neocentromere
JOHE46280/KS579	CNBG_4461_2_Fwd	CCAAACTCGTTTCAGGAGGA	Genes in neocentromere
JOHE46281/KS580	CNBG_4461_2_Rev	TTCTTTATTTGGCCCACAGG	Genes in neocentromere
JOHE46282/KS581	CNBG_1429_1_Fwd	GTCCTACGAGCTTCCTGACG	Genes in neocentromere
JOHE46283/KS582	CNBG_1429_1_Rev	GCAGACTCGAGACCAAGGAG	Genes in neocentromere
JOHE46284/KS583	CNBG_1429_2_Fwd	CGGTCAAGTCATCACCATTG	Genes in neocentromere
JOHE46285/KS584	CNBG_1429_2_Rev	AGCAGACTCGAGACCAAGGA	Genes in neocentromere
JOHE46286/KS585	CNBG_1429_3_Fwd	GGAGCGTGGTTACCTCTTCA	Genes in neocentromere
JOHE46287/KS586	CNBG_1429_3_Rev	TACGACGAGTCTGGTCCCTC	Genes in neocentromere
JOHE46288/KS587	CNBG_1429_4_Fwd	GCTCAAGATTTAGCGACGAA	Genes in neocentromere
JOHE46289/KS588	CNBG_1429_4_Rev	ACTCCTTCACAGCTTCAGGCA	Genes in neocentromere
JOHE46562/KS619	10-7_phusion1_Fwd	AACTAACACGCCTACCTGCC	Chromosome fusion Chr10-7
JOHE46563/KS620	10-7_phusion1_Rev	GTCAGAGACGATGTAGGCGG	Chromosome fusion Chr10-7
JOHE46566/KS623	10-1_phusion1_Fwd	TTTTCGCCCCTGGAAGATCC	Chromosome fusion Chr10-1
JOHE46567/KS624	10-1_phusion1_Rev	GGCCGTAGAAGATTCCCTCG	Chromosome fusion Chr10-1
JOHE46570/KS627	10-4_phusion1_Fwd	ACCGAGAAGGTCAAGCAAGG	Chromosome fusion Chr10-4
JOHE46571/KS628	10-4_phusion1_Rev	TGTCGCGGTGAAGAAGACAA	Chromosome fusion Chr10-4
JOHE50412/KS720	D60_UF_Rev	CTCACCATGCCACCGCCACCCATCATCGTTGCGAGTCTGT	MIS12 construct
JOHE50415/KS723	D60_Hyg_Fwd	CGAGCTGTACAAGTAAAGCGGATAACAATTTCACACAGGA	MIS12 construct
JOHE50416/KS724	D60_Hyg_Rev	TTATGGCGAGATGAGCCGACCGCCAGGGTTTTCCCAGTCACGAC	MIS12 construct
JOHE50417/KS725	D60_DF_Fwd	GTCGTGACTGGGAAAACCCTGGCGGTCGGCTCATCTCGCCATAA	MIS12 construct
JOHE50418/KS726	D60_DF_Rev	TGTCCTTCTCGGTGACTTGC	MIS12 construct
JOHE50419/KS727	D60_Nest_Fwd	CGGCATTCATCGTCGTCTCT	MIS12 construct
JOHE50420/KS728	D60_Nest_Rev	TGCCCTTATCGGTGGTTTCG	MIS12 construct
JOHE50546/KS781	D62_UF_Fwd	GGACCTGTGGTGAAGGGTCA	primers to delete CEN9
JOHE50547/KS782	D62_UF_Rev	GTCGTGACTGGGAAAACCCTGGCGTCTCAGGGTTGGGAGGTCAGT	primers to delete CEN9
JOHE50548/KS783	D62_DF_Fwd	TCCTGTGTGAAATTGTTATCCGCTGGGGGCATACAGCCATGGAAT	primers to delete CEN9
JOHE50549/KS784	D62_DF_Rev	CCAGGTAGGGCGTTTCTGTA	primers to delete CEN9
JOHE50588/KS805	Cen9_A_385	ACCGGCAGGGTATACTGTTGTAGCAAAGTTTAGGGGTAGGTTTTAGAGCTAGAAATAG	Guide RNA to delete CEN9
JOHE50589/KS806	Cen9_A_23	ACCGGCAGGGTATACTGTTCTAAGTACAATGTAGGCACTGTTTTAGAGCTAGAAATAG	Guide RNA to delete CEN9
JOHE50694/KS807	62_out_Fwd	GCCTCCAAAAGCAATCGGTG	primers to delete CEN9
JOHE50695/KS808	62_out_Rev	TATACGGTGCGGTCGAGGTA	primers to delete CEN9
JOHE50697/KS810	D60_GFP_Fwd	ACAGACTCGCAACGATGATGGGAGGCGGAGGCGGAGGCAT	MIS12 construct
JOHE50698/KS811	D60_GFP_Rev	GTCGTGACTGGGAAAACCCTGGCGGTACAGCTCGTCCATGCCGT	MIS12 construct
JOHE51078/KS946	10-6_CNBG_10075_1_Fwd	GCGCGATCATTGACCCTAGA	Genes in neocentromere
JOHE51079/KS947	10-6_CNBG_10075_1_Rev	GTCGCAACTTCATGCCAAGG	Genes in neocentromere
JOHE51080/KS948	10-6_CNBG_10075_2_Fwd	ATTCATTCGGTCCAGGCGAG	Genes in neocentromere
JOHE51081/KS949	10-6_CNBG_10075_2_Rev	CCCTTCGGGTATGTGTTGCT	Genes in neocentromere
JOHE51082/KS950	10-5_CNBG_4495_1_Fwd	TGTCCTCTGGCGAAACCATC	Genes in neocentromere
JOHE51083/KS951	10-5_CNBG_4495_1_Rev	GACGCAGAGTCGTCTCGTAG	Genes in neocentromere
JOHE51084/KS952	10-5_CNBG_4495_2_Fwd	ACCTTGACTGCCTGAATCCG	Genes in neocentromere
JOHE51085/KS953	10-5_CNBG_4495_2_Rev	TGGTTTCGCCAGAGGACATC	Genes in neocentromere
JOHE51086/KS954	10-5_CNBG_10450_1_Fwd	GTACGCATTGGGGTTGAGGA	Genes in neocentromere
JOHE51087/KS955	10-5_CNBG_10450_1_Rev	GGCTCCAATAGTGGCCAAGT	Genes in neocentromere
JOHE51088/KS956	10-5_CNBG_10450_2_Fwd	GTGATATTGCTGGCTGCGAC	Genes in neocentromere
JOHE51089/KS957	10-5_CNBG_10450_2_Rev	AATGGCACGGGAACACTCAA	Genes in neocentromere
JOHE51090/KS958	10-4_CNBG_4379_1_Fwd	GACGAAGGGGAAGGAGATCG	Genes in neocentromere
JOHE51091/KS959	10-4_CNBG_4379_1_Rev	CCACCACCTATGGTCACACC	Genes in neocentromere
JOHE51092/KS960	10-4_CNBG_4379_2_Fwd	CCGTTCGCCATCTTTGTTGG	Genes in neocentromere
JOHE51093/KS961	10-4_CNBG_4379_2_Rev	AGGATTGCATCACCGCAGAA	Genes in neocentromere
JOHE51094/KS962	Cen9_CNBG_5685_1_Fwd	CTTGGCTGCATGTCATGATGG	Genes in neocentromere
JOHE51095/KS963	Cen9_CNBG_5685_1_Rev	GGGTTTAACGGCAACCAAAC	Genes in neocentromere
JOHE51096/KS964	Cen9_CNBG_5685_2_Fwd	CTCATAGGGCTTGCGGTTGT	Genes in neocentromere
JOHE51097/KS965	Cen9_CNBG_5685_2_Rev	TCCATGCGTTACTCTCCTCC	Genes in neocentromere
JOHE51098/KS966	Cen9_CNBG_5684_1_Fwd	TGACGTTTGCCTGTCAACAAC	Genes in neocentromere
JOHE51099/KS967	Cen9_CNBG_5684_1_Rev	GAGCAGTCGCCATTTTCGAG	Genes in neocentromere
JOHE51100/KS968	Cen9_CNBG_5684_2_Fwd	CATACCGCGCCTCTTCAGTC	Genes in neocentromere
JOHE51101/KS969	Cen9_CNBG_5684_2_Rev	AAGCCATGGCCGATTGAGTA	Genes in neocentromere
JOHE51102/KS970	Cen9_CNBG_4377_1_Fwd	ACGTCCGTGTTGCTTGGCTTA	Genes in neocentromere
JOHE51103/KS971	Cen9_CNBG_4377_1_Rev	CTGAGAGAAGGTGCAAGCAGCA	Genes in neocentromere
JOHE51237/KS1041	CEN9_167_CNBG_9613_Fwd	CGAGATTGTTCTGCGCATGG	Genes in neocentromere
JOHE51238/KS1042	CEN9_167_CNBG_9613_Rev	ATGTCCTTTTGGCCATCGGT	Genes in neocentromere
JOHE51239/KS1043	CEN9_167_CNBG_5689_Fwd	CCGTGGAGAGGCTTGGAAAT	Genes in neocentromere
JOHE51240/KS1044	CEN9_167_CNBG_5689_Rev	TGCCGAAGTCGACACCTATC	Genes in neocentromere
JOHE51241/KS1045	CEN9_157_CNBG_5690_Fwd	TAACCTGCATCACGAGTCGG	Genes in neocentromere
JOHE51242/KS1046	CEN9_157_CNBG_5690_Rev	TCTACTGGCGAAAACCCGAG	Genes in neocentromere
JOHE51243/KS1047	CEN9_CNBG_5687_Fwd	GAGCAGATCTTTCGGTGGG	Genes in neocentromere
JOHE51244/KS1048	CEN9_CNBG_5687_Rev	GAGAGAAGGCTGCGGATGA	Genes in neocentromere
JOHE51245/KS1049	NeoCEN10-RNA-expression_control_Fwd	GGCCTTGCCCTTCACGATAA	Genes in neocentromere
JOHE51246/KS1050	NeoCEN10-RNA-expression_control_Rev	AGAAGGCTCAGCTCGTTGTC	Genes in neocentromere
JOHE51247/KS1051	NeoCen10-7_4372_Fwd	CGCCCACTTTGGGACATAGA	Genes in neocentromere
JOHE51248/KS1052	NeoCen10-7_4372_Rev	GCTCTTCCGCCCTGAGTATG	Genes in neocentromere
JOHE51249/KS1053	NeoCen10-7_4373_Fwd	TTTCGAGCCACAGAGGTCAC	Genes in neocentromere
JOHE51250/KS1054	NeoCen10-7_4733_Rev	ACACAATCAACAGTGGCGGA	Genes in neocentromere
JOHE51251/KS1055	NeoCen10-7_4370_Fwd	ATCTCATCACAACACGCCGA	Genes in neocentromere
JOHE51252/KS1056	NeoCen10-7_4730_Rev	CATCGCGCAAAACAGGAACA	Genes in neocentromere

For each primer, the lab identifier, purpose, and sequence are shown.

Supplementary Table 2. Strains used in this study.

Heitman lab ID	Name	Strain	Parental strain	Selection cassette	Reference
20096	KS1	R265 (Wild-type)	-	-	Fraser et al (2005)
20097	KS2	*cen10* △-A	R265	NAT	This study
20098	KS3	*cen10* △-B	R265	NAT	This study
20099	KS4	*cen10* △-C	R265	NAT	This study
20100	KS5	*cen10* △-D	R265	NEO	This study
20101	KS6	*cen10* △-E	R265	NAT	This study
20102	KS7	*cen10* △-F	R265	NAT	This study
20103	KS8	*cen10* △-G	R265	NAT	This study
20104	KS9	*cen10* △-A-S1	KS2	NAT	This study
20105	KS10	*cen10* △-A-L1	KS2	NAT	This study
20106	KS11	*cen10* △-B-S1	KS3	NAT	This study
20107	KS12	*cen10* △-B-S2	KS3	NAT	This study
20108	KS13	*cen10* △-B-S3	KS3	NAT	This study
20109	KS14	*cen10* △-B-L1	KS3	NAT	This study
20110	KS15	*cen10* △-B-L2	KS3	NAT	This study
20111	KS16	*cen10* △-C-S1	KS4	NAT	This study
20112	KS17	*cen10* △-C-S2	KS4	NAT	This study
20113	KS18	*cen10* △-C-S3	KS4	NAT	This study
20114	KS19	*cen10* △-C-L1	KS4	NAT	This study
20115	KS20	*cen10* △-C-L2	KS4	NAT	This study
20116	KS21	*cen10* △-E-S1	KS6	NAT	This study
20117	KS22	*cen10* △-E-S2	KS6	NAT	This study
20118	KS23	*cen10* △-E-S3	KS6	NAT	This study
20119	KS24	*cen10* △-E-L1	KS6	NAT	This study
20120	KS25	*cen10* △-E-L2	KS6	NAT	This study
20121	KS26	*cen9* △-A	R265	NAT	This study
20122	KS27	*cen9* △-B	R265	NAT	This study
20123	KS28	*cen9* △-C	R265	NAT	This study
20124	KS29	*cen9* △-D	R265	NAT	This study
20125	KS30	*cen9* △-E	R265	NAT	This study
20126	KS31	*cen9* △-F	R265	NAT	This study
20126	KS32	R265 MIS12	R265	NAT/NEO	This study
20126	KS33	*cen10* △-A MIS12	KS2	NAT/NEO	This study
20126	KS34	*cen10* △-B MIS12	KS3	NAT/NEO	This study
20126	KS35	*cen10* △-C MIS12	KS4	NAT/NEO	This study
20126	KS36	*cen10* △-D MIS12	KS5	NAT/NEO	This study
20126	KS37	*cen10* △-E MIS12	KS6	NAT/NEO	This study
20126	KS38	R265 CENPC	R265	NAT/NEO	This study
20126	KS39	*cen9* △-A CENPC	KS26	NAT/NEO	This study
20126	KS40	*cen9* △-B CENPC	KS27	NAT/NEO	This study
20126	KS41	*cen9* △-C CENPC	KS28	NAT/NEO	This study
20126	KS42	*cen9* △-D CENPC	KS29	NAT/NEO	This study
20126	KS43	*cen9* △-E CENPC	KS30	NAT/NEO	This study

For each strain used in this study, the lab strain identifier, description, and parental strain are indicated.

Supplementary Table 3. Neocentromeric regions are expressed in the wild-type strain.

	Gene	Gene ID	FPKM value	Present after chromosome fusion
*cen9*Δ-A	Escrt-II complex subunit (VPS25)	CNBG_5690	36.986	
	Iron regulator 1	CNBG_9614	60.887352	
*cen9*Δ-B	Xylosylphosphotransferase	CNBG_5687	77.018387	
	Transglycosylase SLT domain-containing protein	CNBG_9613	68.994972	
	Glutamate synthase (NADPH/NADH)	CNBG_5689	47.843288	
*cen9*Δ-C	Xylosylphosphotransferase	CNBG_5687	77.018387	
	Transglycosylase SLT domain-containing protein	CNBG_9613	68.994972	
	Glutamate synthase (NADPH/NADH)	CNBG_5689	47.843288	
*cen9*Δ-D	Transitional endoplasmic reticulum ATPase	CNBG_5683	261.714935	
	Derlin-2/3	CNBG_5685	38.725452	
*cen9*Δ-E	Xylosylphosphotransferase	CNBG_5687	77.018387	
	Transglycosylase SLT domain-containing protein	CNBG_9613	68.994972	
	Glutamate synthase (NADPH/NADH)	CNBG_5689	47.843288	
*cen9*Δ-F	Xylosylphosphotransferase (XPT1)	CNBG_5687	77.018387	
*cen10*Δ-A	*CENPC/MIF2*	CNBG_4461	80.212288	
	Hypothetical protein	CNBG_4462	76.699188	
	Serine/threonine-protein phosphatase 2A activator 2*(RRD2)*	CNBG_9459	61.127243	
	Hypothetical protein	CNBG_4366	13.426547	
	Hypothetical protein	CNBG_4365	279.7435	
*cen10*Δ-B	*CENPC/MIF2*	CNBG_4461	80.212288	
	Hypothetical protein	CNBG_4462	76.699188	
*cen10*Δ-C	*CENPC/MIF2*	CNBG_4461	80.212288	
	Hypothetical protein	CNBG_4462	76.699188	
	Serine/threonine-protein phosphatase 2A activator 2*(RRD2)*	CNBG_9459	61.127243	
	Hypothetical protein	CNBG_4366	13.426547	
	Hypothetical protein	CNBG_4365	279.7435	
*cen10*Δ-D	Ser/Thr protein kinase	CNBG_4379	23.199852	
*cen10*Δ-E	Hypothetical protein	CNBG_10450		
	Hypothetical protein	CNBG_4495	4.149051	
*cen10*Δ-F	Hypothetical protein	CNBG_4383	54.773762	
	Hypothetical protein	CNBG_10075		
	Hexokinase (HXK1)	CNBG_4382	181.213837	
*cen10*Δ-G	High osmolarity signaling protein (SHO1)	CNBG_4373	162.575226	
	Hypothetical protein	CNBG_4372	30.983101	
	Hypothetical protein	CNBG_4371		
	Hypothetical protein	CNBG_4370	62.656879	
Housekeeping genes	Actin	CNBG_1429	1871.39	
	Histone H3	CNBG_5663	992.68	
	Tubulin beta chain	CNBG_3361	2070.41	
	Tubulin alpha-1A	CNBG_0187	1354.83	
	CENPA	CNBG_0491	139.08	
Median	Median expression of all genes on chromosome 9		96.8559645	
	Median expression of all genes on chromosome 10		96.29	
Subtelomeric regions	10R	CNBG_6141	13.25	X
	10R	CNBG_6142	17.76	X
	10R	CNBG_6143	56.12	X
	10R	CNBG_6144	28.00	✓
	10L	CNBG_4495	4.15	Present at other side of chromosome
	10L	CNBG_4494	5.68	Present at other side of chromosome
	1R	CNBG_10308		X
	1R	CNBG_3720	8.57	✓
	1L	CNBG_10000		Present at other side of chromosome
	1L	CNBG_2934	0.42	Present at other side of chromosome
	4R	CNBG_10211		X
	4R	CNBG_10105		X
	4R	CNBG_6174	189.80	✓
	4L	CNBG_10291		Present at other side of chromosome
	4L	CNBG_0541	31.67	Present at other side of chromosome
	7R	CNBG_10214		X
	7R	CNBG_10183		X
	7R	CNBG_2029	71.86	X
	7R	CNBG_2030	6.63	X
	7R	CNBG_2031	7.59	X
	7R	CNBG_2032	20.30	X
	7R	CNBG_2033	16.99	X
	7R	CNBG_2034	44.50	X
	7R	CNBG_2036	37.45	✓
	7L	CNBG_2485	0.23	Present at other side of chromosome
	7L	CNBG_2484	75.63	Present at other side of chromosome

Expression levels of genes where neocentromeres formed in the *cen*Δ mutants were analyzed in the R265 wild-type strain. Previously generated RNA sequencing data were remapped to the R265 reference genome, and the expression levels (FPKM) were analyzed for the native genes in each region wherein a neocentromere was formed in the *cen*Δ mutants [35]. Expression analysis of several housekeeping genes was included for control purposes, and the median RNA expression level of all genes located on chromosomes 9 and 10 are listed. Expression levels of genes located in the subtelomeric regions were also analyzed.

Supplementary Table 4. Neocentromeres are not enriched with transposable elements.

Isolate	Chromosome/scaffold	% Identical matches	Alignment length	# Mismatches	# Gap openings	Alignment in query		Alignment in subject		Evalue	Bitscore
						Start (bp)	End (bp)	Start (bp)	End (bp)		
WT	scaffold3.10	100	4537	0	0	1	4537	115939	120475	0	8379
WT	scaffold3.10	100	3179	0	0	1	3179	390605	393783	0	5871
cen10Δ-A	NODE_39	100	4537	0	0	1	4537	17760	13224	0	8379
cen10Δ-A	NODE_11	100	3179	0	0	1	3179	242270	245448	0	5871
cen10Δ-B	NODE_42	100	4537	0	0	1	4537	17765	13229	0	8379
cen10Δ-B	NODE_10	100	3179	0	0	1	3179	250468	253646	0	5871
cen10 Δ-C-L1	NODE_42	100	4537	0	0	1	4537	115954	120490	0	8379
cen10 Δ-C-L1	NODE_10	100	3179	0	0	1	3179	266017	262839	0	5871
cen10 Δ-C-L2	NODE_59	100	4537	0	0	1	4537	61353	65889	0	8379
cen10 Δ-C-L2	NODE_26	100	3179	0	0	1	3179	242325	245503	0	5871
cen10Δ-E	NODE_41	100	4537	0	0	1	4537	25951	21415	0	8379
cen10 Δ-E	NODE_9	100	3179	0	0	1	3179	242271	245449	0	5871

To exclude the possibility that transposable elements were deposited into the neocentromeres, BlastN searches in a database with *de novo* genome assemblies of *cen10* Δ-A, *cen10* Δ-B, *cen10* Δ-C, and *cen10* Δ-E were performed. As input the homologous wild-type sequence of the chromosomal location of the neocentromeres was used. All neocentromeres of the tested *cen10* Δ mutants have the same length as the homologous sequence in the wild-type.

Supplementary Table 5. Genes located in subtelomeric regions of chromosomes 1, 4, 7, and 10.

Sub telomeric region	Gene ID	Position of gene based on telomere	Chromosome location	Putative function	Present after chromosome fusion	*C. neoformans* homolog	Putative function of *C. neoformans* homolog	Synthenic	*C. neoformans* homolog present in knockout library
10R	CNBG_6141	1	10:808,557-811,688	Hypothetical protein	X	CNAG_05665	Hypothetical protein	✓	X
10R	CNBG_6142	2	10:805,256-806,895	Branched-chain-amino-acid transaminase	X	CNAG_05664	Branched-chain-amino-acid transaminase	✓	Madhani 2015
10R	CNBG_6143	3	10:800,576-803,649	Cell wall integrity protein scw1	X	CNAG_05663	Cell wall integrity protein scw1	✓	Madhani 2015
10R	CNBG_6144	4	10:796,089-798,416	Sugar transporter	✓	CNAG_05662	Polyol transporter protein 1 PTP1	✓	Madhani 2008 and Madhani 2015
10L	CNBG_4495	1	10:601-3,764	Predicted protein	Present at other side of chromosome	Unique to *C. deuterogattii*	ND	ND	ND
10L	CNBG_4494	2	10:4,399-5,971	Hypothetical protein	Present at other side of chromosome	No homolog in *C. neoformans*	ND	ND	ND
1R	CNBG_10308	1	1:2,206,312-2,207,306	ND	X	ND	ND	ND	ND
1R	CNBG_3720	2	1:2,204,102-2,205,682	Hypothetical protein	✓	No homolog in *C. neoformans*	ND	ND	ND
1L	CNBG_10000	1	1:3,548-5,589	ND	Present at other side of chromosome	ND	ND	ND	ND
1L	CNBG_2934	2	1:6,225-6,818	Hypothetical protein	Present at other side of chromosome	No homolog in *C. neoformans*	ND	ND	ND
4R	CNBG_10211	1	1,740,094-1,740,783	ND	X	ND	ND	ND	ND
4R	CNBG_10105	2	4:1,737,708-1,739,785	ND	X	ND	ND	ND	X
4R	CNBG_6174	3	4:1,734,189-1,736,937	Transketolase	✓	CNAG_00866	Transketolase, transketolase, variant	✓	Madhani 2016
4L	CNBG_10291	1	4:3,225-4,992	ND	Present at other side of chromosome	ND	ND	ND	ND
4L	CNBG_0541	2	4:6,010-9,384	Hypothetical protein	Present at other side of chromosome	CNAG_00010	Cation transporter	✓	X
7R	CNBG_10214	1	7:1,241,250-1,242,246	ND	X	ND	ND	ND	ND
7R	CNBG_10183	2	7:1,240,383-1,240,898	ND	X	ND	ND	ND	ND
7R	CNBG_2029	3	7:1,237,355-1,239,923	Hypothetical protein	X	CNAG_06967	Phytase	✓	Madhani 2015
7R	CNBG_2030	4	7:1,235,767-1,237,137	Metabolite transporter	X	Unique to *C. deuterogattii*	ND	ND	ND
7R	CNBG_2031	5	7:1,233,786-1,234,252	Hypothetical protein	X	CNAG_06966	Alkaline phosphatase D	✓	Madhani 2016
7R	CNBG_2032	6	7:1,230,857-1,232,783	UDP-galactopyranose mutase	X	CNAG_07752	UDP-galactopyranose mutase	✓	Madhani 2015
7R	CNBG_2033	7	7:1,228,774-1,230,252	Hypothetical protein	X	CNAG_06994	Hypothetical protein	✓	Madhani 2008
7R	CNBG_2034	8	7:1,226,338-1,227,719	Hypothetical protein	X	CNAG_06993	Hypothetical protein	✓	Madhani 2015
7R	CNBG_2036	9	7:1,221,116-1,223,113	Siderophore iron transporter mirB	✓	CNAG_07751	Siderophore iron transporter mirB	✓	Madhani 2016
7L	CNBG_2485	1	7:1,489-3,173	Hypothetical protein	Present at other side of chromosome	CNAG_03097	Hypothetical protein	✓	Madhani 2016
7L	CNBG_2484	2	7:3,868-4,780	Predicted protein	Present at other side of chromosome	CNAG_03098	Hypothetical protein	✓	X

We have indicated whether each gene located in the subtelomeric regions was lost in the chromosomal fusion of the large-colony *cen10* Δ mutants. For each gene in the subtelomeric region of chromosome 1, 4, 7, and 10 several characteristics as the chromosomal location, putative function, and the presence of putative *C. neoformans* homologs in existing mutant libraries are indicated. There is no correlation between the loss of genes with or without predicted function.